Nondestructive Evaluation of Zirconium Phosphate Bonded Silicon Nitride Radomes

by

Jonathan A. Medding

Thesis submitted to the Faculty of the
Virginia Polytechnic Institute and State University
in partial fulfillment of the requirements for the degree of

MASTER OF SCIENCE
IN
MATERIAL SCIENCE AND ENGINEERING

APPROVED:

J.C. Duke, Jr., Chair

E.G. Henneke

S.L. Kampe

December 17, 1996
Blacksburg, Virginia

Keywords: NDE, Ultrasonic, Silicon Nitride, Radome, Porosity

NONDESTRUCTIVE EVALUATION OF ZIRCONIUM PHOSPHATE BONDED SILICON NITRIDE RADOMES

by

Jonathan A. Medding

Dr. J.C. Duke, Jr., Chairman

Material Science and Engineering

(ABSTRACT)

The performance advances of radar-guided missiles have created a need for radome materials with improved strength, toughness, and thermal shock capabilities. Zirconium phosphate bonded silicon nitride (Zr-PBSN), which has a low and thermally stable dielectric constant, high rain erosion resistance and a low-cost processing method, has been developed for radome applications in advanced tactical missiles. Pressureless sintering reduces processing costs, but is untried for radome manufacturing. The tendency for catastrophic failure requires that each radome fabricated with this material/method be inspected for defects prior to use. Visible, thermographic and ultrasonic nondestructive evaluation (NDE) methods have been tested with Zr-PBSN discs containing fabricated flaws likely to be present in a radome.

Ultrasonic C-scanning using a 0.25" diameter, 15 MHz focused transducer with a pulse-echo configuration was clearly superior at detecting cracks, delaminations, impurities, voids and porosity variation. A method for determining local porosity via the longitudinal elastic wave velocity was developed and can be incorporated into an ultrasonic scanning system. A system that uses a computer to perform all motion control, data acquisition, and data manipulation, but requiring a skilled operator for scan setup and interpretation of the data has been proposed.

ACKNOWLEDGEMENT

The author of this thesis would like to acknowledge Dr. John Liu from the Material Characterization Group at the Naval Surface Warfare Center, Carderock Division, for guidance, support and funding provided. Dr. Salient Chatterjee, from the Material Science Corporation has acted as our corporate sponsor. Dr. Inna Talmy, Curtis Martin, Dr. Jim Zackowski and Dr. Eric Wuchina from the Ceramic Group at the Naval Surface Warfare Center, Carderock Division, were very helpful with providing material information and fabrication of samples. As advisor and chair of the defense committee, Dr. John Duke, Jr. has been a key provider of guidance and support.

LIST OF FIGURES PAGE

LIST OF TABLES PAGE

TABLE OF CONTENTS PAGE

INTRODUCTION AND LITERATURE REVIEW

A new ceramic material has been developed for advanced radar guided missile radomes. This material has mechanical and dielectric properties that are equal to or better than existing radome materials, but at a significant cost benefit compared to other high performance materials. The major cost benefits are derived from the production method, which utilizes a net shape, pressureless sintering technique. The reliability of this process has not yet been proven therefore a means to check radome integrity is necessary so that failure will not occur during the service life radome. This thesis describes a project aimed at developing a radome nondestructive evaluation (NDE) system for this new material.

Radar units are often expected to operate in environments that are physically damaging to the components of the system. In these situations a radome is used to protect the radar unit from its environment, while still allowing the electromagnetic microwaves to propagate through. Radome materials currently used in advanced tactical missiles are slip cast fused silica (SCFS) and Pyroceram 9606^{TM} ($2MgO{\cdot}2Al_2O_3{\cdot}5SiO_2$, cordierite) [1]. While SCFS has excellent dielectric properties for radome applications, the relatively low strength and rain erosion resistance of this material limit its future application. Pyroceram 9606^{TM} is more rain erosion resistant than SCFS, but is not as dielectrically stable with temperature.

Future classes of advanced tactical missiles will require new radome materials to meet stringent requirements arising from greater speeds and longer flight times. The material must be stable up to 1400°C with a low and thermally stable dielectric constant, low coefficient of thermal expansion (CTE), and high thermal shock and rain erosion resistance [1] as shown in Table I.

Table I. Radome material specifications and zirconium-phosphate (30%) bonded silicon nitride properties.

	REQUIRED	ZR - PBSN
Service Temperature	UP TO 1400°C	1500°C
Dielectric Constant	< 9.0 (5.0 preferred)	4.98
Temperature variation of Dielectric Constant to 1260°C	< 7.0%	6.5%
Loss Tangent to 1260°C	< 0.1	0.0031
Bending Strength(4 point)	> 35 MPa (5 KSi)	71.6 MPa

Development of future radome materials is directed both toward improvement of the mechanical properties of SCFS and identification of new candidate ceramic materials. For example, materials in the system Si_3N_4-BN-SiO_2 (Nitroxyceram) have potential to be nearly as good as SCFS dielectrically and at least as good if not better than Pyroceram 9606^{TM} in erosion resistance [1]. A disadvantage is this material requires expensive processing techniques such as hot iso-static pressing (HIP). A promising candidate ceramic material based on monoclinic celsian ($BaO{\cdot}Al_2O_3{\cdot}2SiO_2$) was developed at the Naval Surface Warfare Center (NSWC)[1]. Celsian based ceramics have the potential to be manufactured in radome shapes by pressureless sintering, which offers a significant cost benefit compared to HIP ceramics.

Another promising ceramic material based on phosphate bonded silicon nitride (PBSN) which also utilizes pressureless sintering was developed at NSWC. Phosphate binders have been used for many years in manufacturing conventional refractories.[2] The method is based on formation of strong metal phosphate bonds in a ceramic body as a result of low temperature (room temperature to a few hundred degrees C) chemical reactions between selected oxides and phosphoric acid or other phosphorous containing compounds. Phosphate binding can be particularly useful for the preparation of non-oxide ceramics. It can provide a means for low cost, low temperature processing for applications where very high strength potential is not required. Although phosphate

bonding does not result in fully dense high strength non-oxide ceramics, it allows exploitation of their other unique properties, such as dielectric properties suited for advanced radome applications.

Phosphates can be formed in ceramics by direct reaction between selected oxides and phosphoric acid (H_3PO_4). Ceramics composed of Al-, B-, Si, and Zr-PBSN have been evaluated at NSWC [3,4]. The ceramics were prepared by mixing the oxide and phosphoric acid at room temperature and then adding this mixture to Si_3N_4 to achieve a 25-30 vol% mixture of metal-phosphate and Si_3N_4. The material was then fired at 900°C after cold iso-static pressing (CIP) at 420 MPa (60Ksi). The phosphoric acid reacts with the oxides at low temperatures (250°C for Zr [5]) to form the metal-phosphates *in situ*. The metal-phosphates reacted with the Si_3N_4 at high temperatures to achieve pressureless sintering.

Of all materials considered, Zirconium-PBSN was chosen as the best possible radome material. The properties [6] pertinent to radome applications of Zr-PBSN (30 vol% Zirconium phosphate [ZrP_2O_7]) are listed in Table I. This material had a coefficient of thermal expansion (CTE) of $2.5*10^{-6}$/°C in the temperature range of 25 - 850°C. Net shrinkage upon firing was less than 1%, which makes this material suitable for net shape processing applications, however the apparent porosity, determined by the Archimedes method, was 16%, which limits the strength and toughness of the material.

Residual zirconia (ZrO_2), detected by x-ray diffraction(XRD) is present in fired Zr-PBSN in small amounts (less than 3 wt%). Zirconia has a large dielectric constant and its presence is minimized by using a very fine grade of zirconia (22 g/cm^3 specific surface area) to facilitate its reaction with the phosphoric acid. The effects of using different grades of Zirconia can be seen in Table II. The effects of residual Zirconia on the dielectric constant can be seen in Fig. 1.

Zirconium phosphate is stable up to 1500°C, yet thermogravimetric analysis (TGA) shows weight loss (Fig. 2) beginning at 1100°C [6]. This is explained by the presence of silicon phosphate ($Si_3(PO_4)_4$), which begins to decompose at 900°C. The presence of crystalline

Table II. A table showing the effects of starting Zirconia particle surface area and residual Zirconia after processing.

GRADE	SURFACE AREA (g/cm^3)	RESIDUAL ZRO_2 (wt%)
E101	22	2.4
762/01	5	6.2
760/01	2.5	7.8

silicon phosphate was confirmed by XRD [6] (Fig. 3), although the majority of the silicon phosphate is believed to be amorphous and thus non-detectable [1] by XRD. Silicon phosphate is formed by the reaction of the phosphoric acid and silica (SiO_2), which is present on the surface of the silicon nitride particles [6].

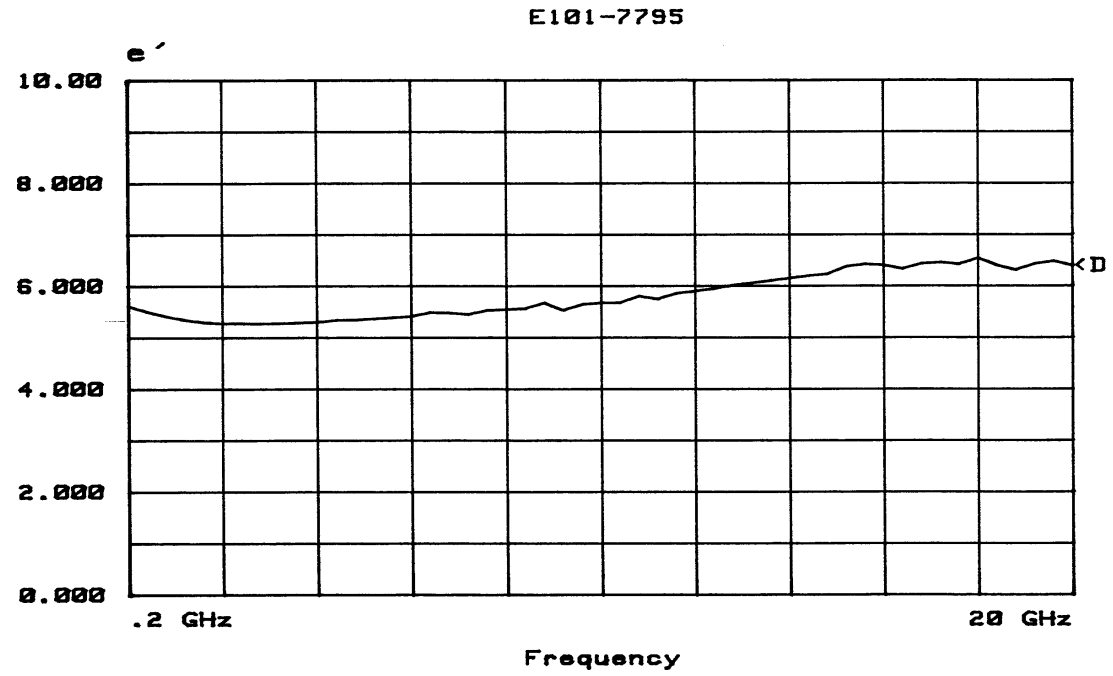
E101-7795
e´
10.00
8.000
6.000
4.000
2.000
0.000
.2 GHz
20 GHz
Frequency
D

[a]

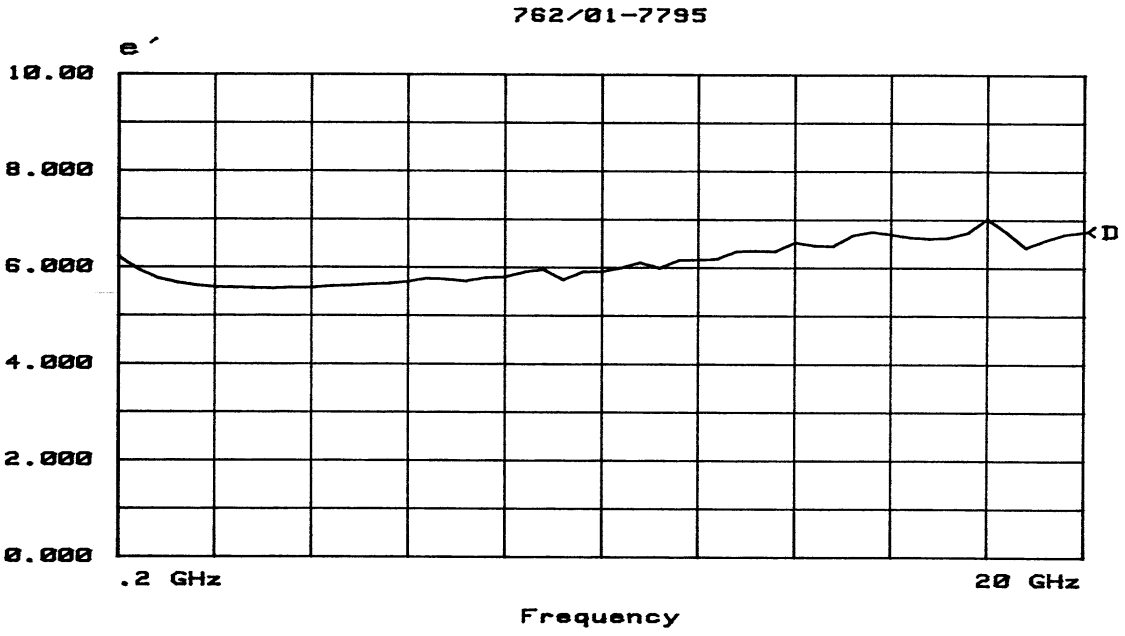
762/01-7795
e´
10.00
8.000
6.000
4.000
2.000
0.000
.2 GHz
20 GHz
Frequency
D

[b]

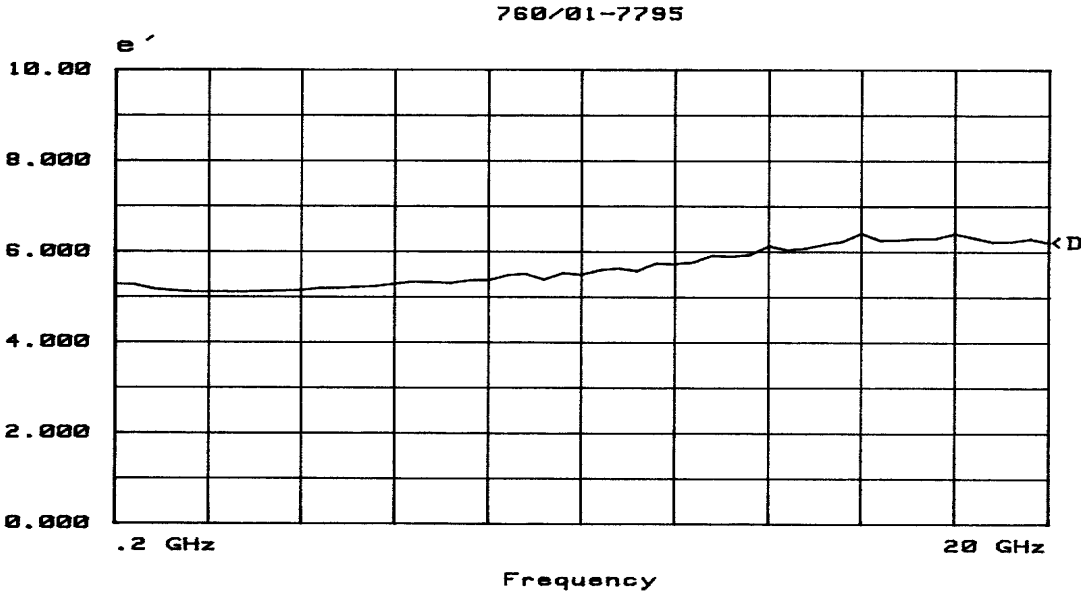

[c]

Figure 1. Graphs of dielectric constant versus frequency for three different amounts of residual Zirconia, [a] 2.4 wt%, [b] 6.2 wt%, [c] 7.8 wt%.

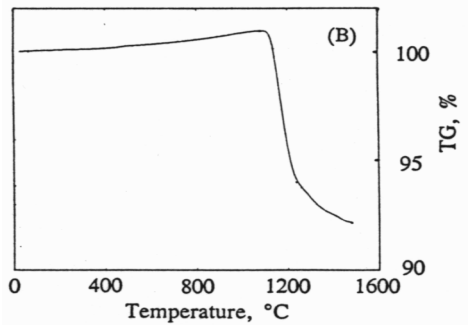

Figure 2. The TGA curve for Si_3N_4/ZrP_2O_7. Zirconium phosphate is stable to 1500°C which does not correspond to the sharp loss of weight at 1100°C. The loss of silicon phosphate, which forms from SiO_2 present on the surface of the silicon nitride particles, is responsible for the weight loss.

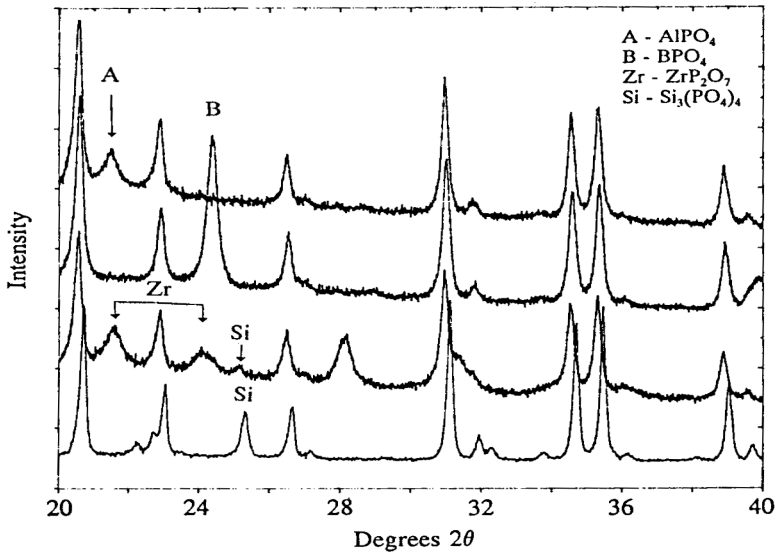

Figure 3. The X-Ray Diffraction Pattern for Zr-PBSN, which is located 3rd from the top showed the presence of crystalline silicon phosphate. The significant weight loss observed in the TGA does not correspond to the amount of silicon phosphate shown by XRD, thus it is believed that the majority of silicon phosphate is amorphous and undetectable by XRD.

Zr-PBSN was found to have excellent resistance to thermal shock. The change in strength was less than 10 percent for thermal shocks of 1000 and 1125°C. These temperatures were chosen to simulate possible service environments of tactical missile radomes [5]. This behavior is explained by the softening of the silicon phosphate, which allows accommodation of stresses caused by rapid heating and cooling. This characteristic is extremely important for radome applications due to the significant temperature gradient which occurs across the thickness of the dome [5] while in operation. The softening of the silicon phosphate binder at high temperatures also increases the plasticity of Zr-PBSN. This improves the fracture toughness at high temperatures, which increases the rain erosion resistance.

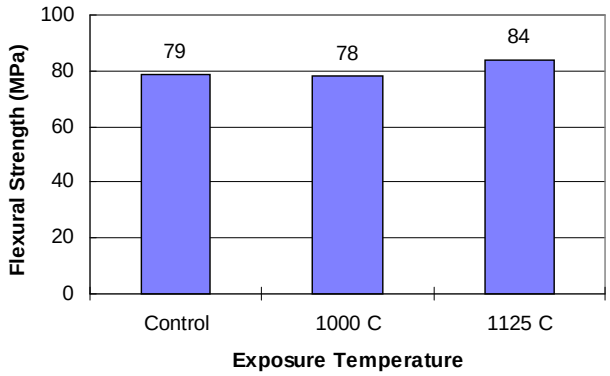

Figure 4. Strength of Zr-PBSN after thermal shock at 1100 and 1125°C. The control sample was left at room temperature.

Zr-PBSN was not degraded by exposures (Fig. 5) to boiling water for one hour, sitting in water for three months at room temperature, or to water vapor for three months [5]. It is suitable for applications in wet or damp environments such as a ship or coastal emplacement.

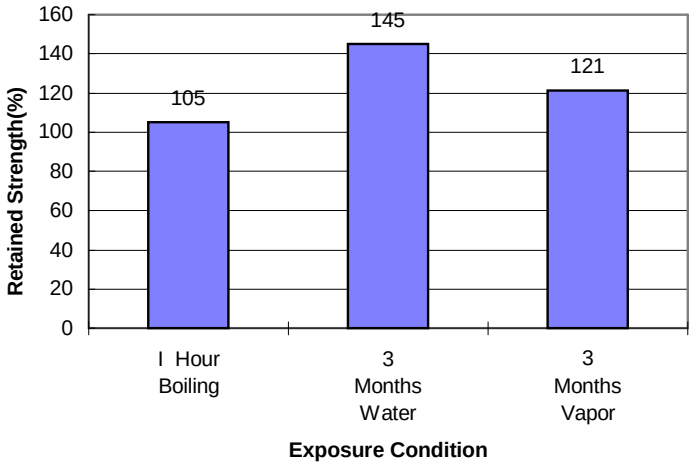

Figure 5. The effects of exposure to various water environments on Zr-PBSN.

As tactical missile capabilities are increased, so are demands on the individual components of the missile system. Zr-PBSN is a material that has been developed for

radome applications which offers improved mechanical and dielectric characteristics compared to existing radome materials with the added benefit of low cost processing. Manufacturing Zr-PBSN components with the radome geometry has not yet been perfected and a methodology for evaluating the fitness of Zr-PBSN radomes for service is required.

NDE APPROACH OVERVIEW

Zirconium phosphate bonded silicon nitride (Zr-PBSN) has mechanical and dielectric properties that offer significant advantages over SCFS, Pyroceram 9606^{TM}, and Celsian for use as a radome material in advanced tactical missiles. Manufacturing Zr-PBSN in the radome shape requires special consideration to avoid creating defects. The difficulty associated with processing Zr-PBSN in a radome shape and the catastrophic nature of failure warrants that every dome be inspected before use. Visible inspection has been the most common method of nondestructive evaluation in manufacturing, but many defects are not easily detectable by visual inspection or are located below the surface and are thus entirely undetectable by this method. Any inspection technique used must detect surface and sub-surface defects yet not diminish the usability of the dome (nondestructive).

It is the goal of this project to develop a system that will perform nondestructive evaluation (NDE) on Zr-PBSN radomes in a manufacturing environment. Before evaluation of various NDE methods can be done the defects which are to be detected must first be specified. There are imperfections in all ceramic materials due to their processing and the point at which an imperfection is considered to be a defect is determined by the loading material is expected to experience under service conditions. Imperfections of concern include porosity (Fig. 6) which consists of microscopic voids,

finely dispersed throughout the material. Cracks are important because they can act as failure sites while in use. Cracks can be divided into categories based on their orientation and location. They can be surface or subsurface depending on whether they exit the surface of the material or are completely contained with in it. Radial cracks are oriented mainly perpendicular to the radome wall while delaminations are oriented parallel to the wall (Figs. 7 and 8). Surface and subsurface versions of both types of crack can exist. Inclusions are macroscopic voids which can act as crack initiation sites as well as affect the dielectric signature of the dome wall. Impurities, which are pieces of foreign matter (Fig. 9), can also affect the dielectric signature of the wall if their dielectric constant is significantly different than that of Zr-PBSN.

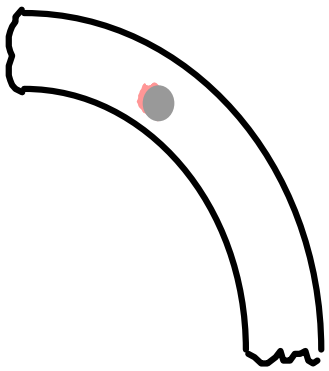

Figure 6. A section of radome with a region of high porosity.

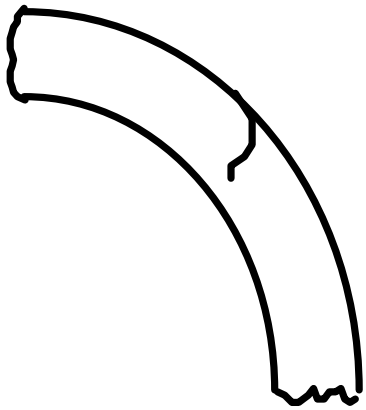

Figure 7. A section of radome with a radial surface crack.

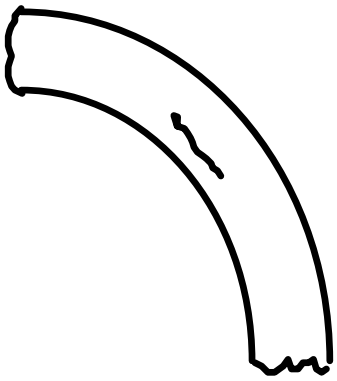

Figure 8 A section of radome with an internal delamination.

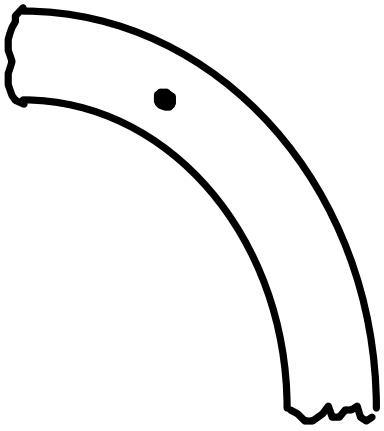

Figure 9. A section of radome with an internal impurity.

The ability to detect imperfections of the specified size in Zr-PBSN is not the only criterion for NDE method selection. There are several other factors which affect the feasibility of any particular method. These include geometrical concerns, the need for immersion in water or other surface preparations, cost of method/equipment, operator involvement, and time necessary for inspection. The ideal method would be able to provide the location and characterize any flaw of interest, have absolutely no effect on the dome itself, cost little compared to the manufacturing cost, be rapid and reliable.

The radome consists of a hollow cone shaped shell. It is axially symmetric and has a constant wall thickness along its length, which is slightly curved (Fig. 10). An inspection method that requires scanning over the surface could be done by taking advantage of the axial symmetry (vertical axis) and scanning in the azimithal direction while stepping in the vertical direction.

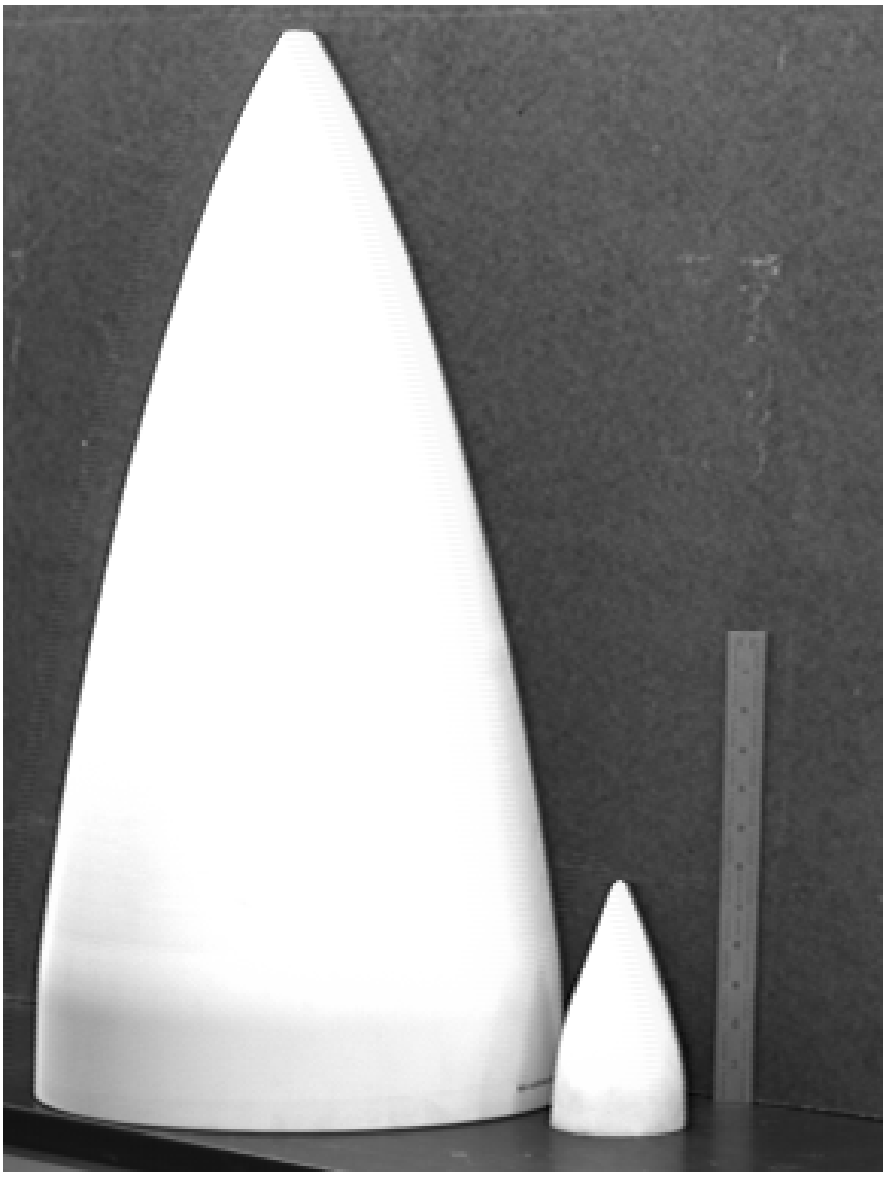

Figure 10. An image showing a full size radome on the left and the small hand-made radome on the right.

Special care would be necessary in regards to keeping the scanning unit perpendicular to the surface being scanned. This can be accomplished by mechanical or computer-control solutions. An NDE method that can analyze the entire dome from a distance, such as visual inspection, an infrared camera or X-ray and film, would overcome the complicated geometric problems that arise in scanning.

Ultrasonic inspection is a common method of NDE for ceramic materials. It requires more interaction with the material than some other methods because it requires some form of couplant that will facilitate wave propagation from the transducer (used to generate the wave) to the material, through which it travels, and back to the recording transducer. The couplant is often water or some gel type material. The interaction of the couplant and the material must not affect the radome permanently. Rolling transducers, which use a visco-elastic coupling material that leaves no residue on the radome surface, could be used but at the cost of resolution due to the imperfect coupling of the soft rubber rolling surface. Another concern is how the presence of residual couplant may affect other inspection techniques. For example microwave inspection will be affected by any water absorbed during an immersion type test due to water's high dielectric constant.

As with all commercial ventures, cost is a factor. The system must be able to detect any imperfection which endangers the functionality of the radome. This often requires a minimum resolution. Some methods have a greater resolution than others due to their nature but generally a method can achieve greater resolution by spending more money. Time is also a factor. If two methods have similar costs at a certain resolution the time for inspection and the ease of use would be deciding factors. Often time and resolution are linked as well. An increase in scanning resolution, for instance results in a longer scanning time, unless money is spent to upgrade the system so that it will scan faster.

Of all the various NDE methods available, there is not likely to be one perfect choice. Budget is certainly a prime concern, but if a less costly method can not detect potentially lethal defects, it is not worth any price. It is possible that more than one method may be necessary to insure total detection. Other factors include operator involvement and time of inspection. Samples have been constructed with fabricated defects to evaluate the candidate NDE methods' abilities to detect defects of interest.

SAMPLE PREPARATION

The first step in the process of selecting NDE methods for Zr-PBSN radomes was to construct sample specimens with imbedded defects that could be used to test the ability of a candidate method to detect flaws of interest. There were two main requirements that had to be met before an NDE method could be considered successful at detecting a flaw. The first was the resolution of the detection method be fine enough to locate defects of some minimum size, below which the defect would not affect the performance of the radome. The second requirement was these same defects must be detectable in a component with radome geometry.

Defects of interest included imperfections commonly encountered in ceramic processing plus those that could result from the manufacturing method of the radome. Imperfections such as cracks, voids and regions of high porosity (due to incomplete packing) are common to ceramic materials. An uneven distribution of Zirconia (ZrO_2) may have little effect on the mechanical properties of the dome, and thus may not normally be of interest, but due to Zirconia's high dielectric constant and loss tangent it could affect the dielectric signature of the radome so that radar performance would be impaired. Dielectric properties are equally important as mechanical properties for

radomes, making Zirconia distribution important. Impurities such as metal, oil, grease and polymers which are present in the manufacturing environment, could have effects on the mechanical and/or dielectric properties of the ceramic as well and their presence must be detectable if they affect a radome's performance. For this purpose, two inch diameter discs were fabricated with flaws purposely manufactured in them (see appendix for details) to evaluate various NDE methods' ability to detect flaws of interest.

The first sample (disc #1) was constructed to be flaw free and it was used as a control. Discs #2 and #3 were made with different grades of Zirconia. Each grade had a different Zirconia particle size. Tests were done to compare the effect of Zirconia particle size on how completely the Zirconia reacted with the phosphoric acid. How the amount of residual Zirconia affected the dielectric constant of the material was also investigated over a range of frequencies.

Disc #4 was constructed so that a region of high porosity was formed by moving powder away from the center of the mold before die pressing. The sample was die pressed and because there was more powder located on the outer edge of the disc than the center (see Fig. 11), the packing in the middle was not as dense as that on the outer portion of the disc. This sample was the only disc not cold iso-static pressed (CIP) after die-pressing. This was done to avoid packing the center region which would remove the zone of high porosity that had been created.

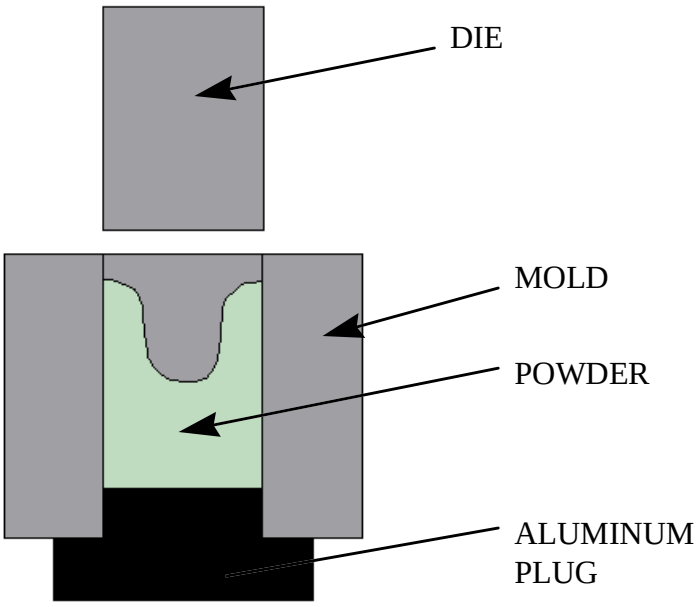

Figure 11. A diagram showing the powder distribution in the mold before die pressing disc # 4. The extra powder on the outer edge of the mold will result in denser packing and thus lower porosity.

Voids were intentionally created in disc #5. An attempt to create voids was made by placing small polymer fillers within the disc which subsequently burned off upon firing. Half of the powder was poured into the mold and lightly packed with the die resulting in a flat surface. Six polymer triangles, shown in Fig 12a., were placed in a circle about the center of the disc (Fig 12b). The rest of the powder was carefully poured into the mold so that the spacing of the polymer triangles would not be altered. The sample was die-pressed, iso-pressed and fired. Upon removal from the oven a large crack running parallel to the disc face was observed roughly in the middle of the specimen, but not corresponding to the interface of the initial powder layer and the addition of the remaining powder (Fig. 13). The crack appeared to exist throughout most of the disc.

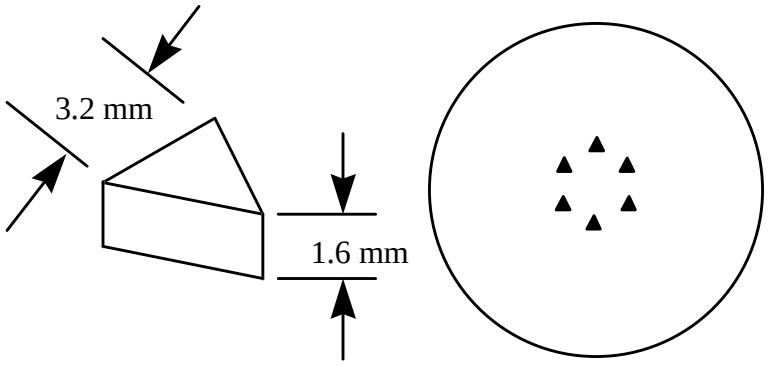

Figure 12. (a) A small polymer triangle used to create voids in disc #5. (b) The arrangement of triangles in disc number five, located at a depth of half the sample height.

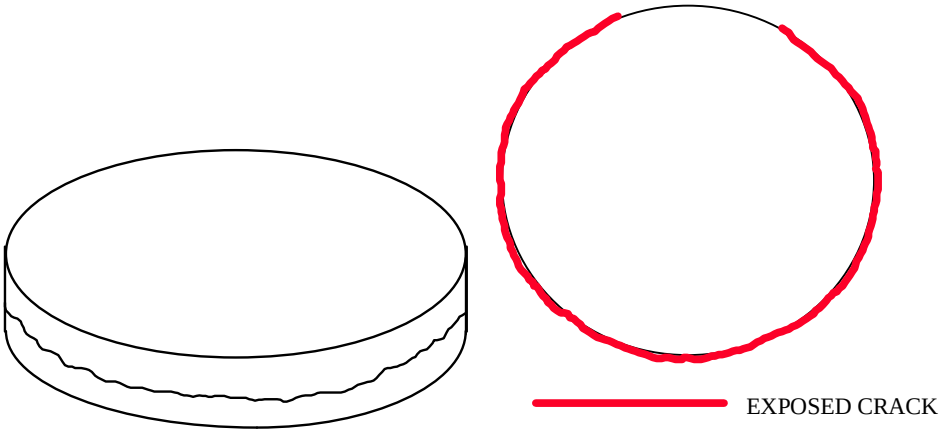

Figure 13. The crack that resulted from firing in disc #5. The vertical location is shown in the left diagram, while the extent of the crack which was detectable from the surface is shown by the right diagram.

Disc #7 was constructed by pouring about half of the powder into the mold and lightly packing with the die. Steel shavings from a milling machine were placed on the surface in a circular area in the center of the disc as shown in Fig. 14. The shavings were roughly 1 mm by 2 to 3 mm in dimension and in the form of ribbon like coils. The shavings were also coated in cutting oil. The rest of the powder was carefully poured into the mold so that the shavings were not moved around too much, and then die-pressed. Upon removal from the mold a crack was observed that was located roughly in

the middle of the disc, parallel to the surface. It extended through roughly one half of the sample (see Fig. 15). It is most likely that this crack was caused by the difference in stress-strain characteristics between the powder and the ribbon like shavings. After release of the pressure the steel shavings were able to exert enough force in their attempt to return to their equilibrium positions that they caused the crack to form. Since it would be nearly impossible to separate the shavings from the powder and certainly impossible to remove all of the cutting oil that coated the shavings, it was decided to try and make use of the good half of the disc and to continue with the CIP and firing. The crack showed no further signs of growth after firing.

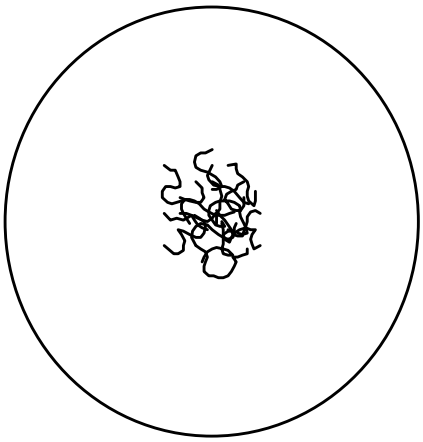

Figure 14. The distribution of steel shavings in disc #7. The shavings were roughly 1 mm by 3 mm in dimension and had curled ribbon-like shapes.

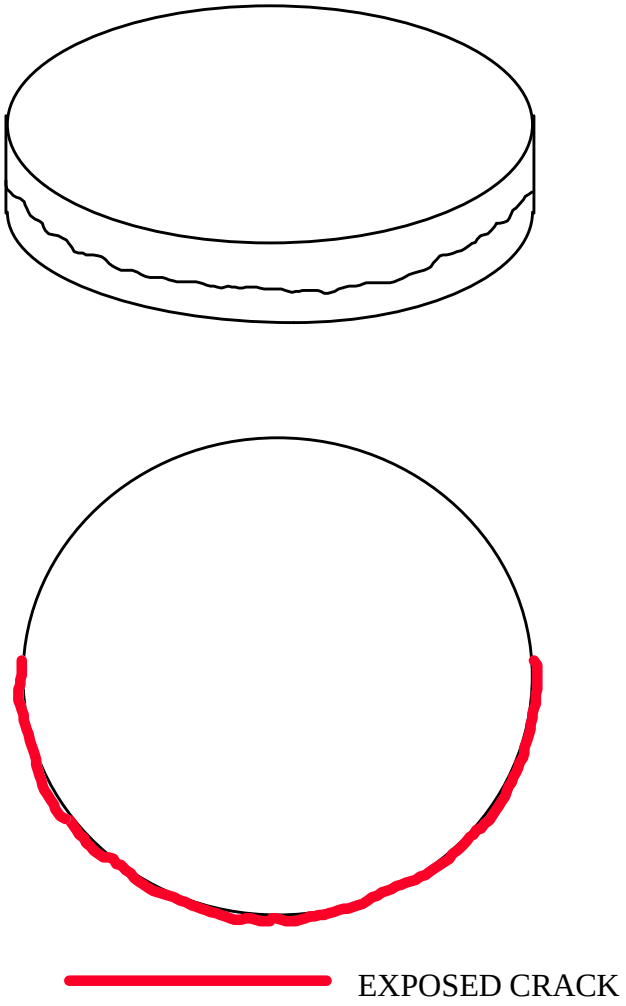

Figure 15. The surface indication of the crack formed in disc #7 after release from the mold.

A vertical surface crack was manufactured into disc #8. A piece of construction paper with dimensions 1.27 cm by 3.81 cm was bent into an “L” shape as shown in Fig 16, and placed on top of the mold plug in the center of the mold. Powder was poured into the mold and die pressed. After removal of the disc from the mold, it was observed that the paper “L” was exposed on one surface (the bottom). The sample was CIP and fired. Upon firing the paper burned away leaving an “L” shaped surface crack. Smaller, “hairline” cracks were observed running from the corners of the manufactured crack to the outer edge of the disc (see Fig. 17). The crack width for these secondary cracks was

observed to decrease as their vertical location increased. The top surface of the disc was completely crack-free.

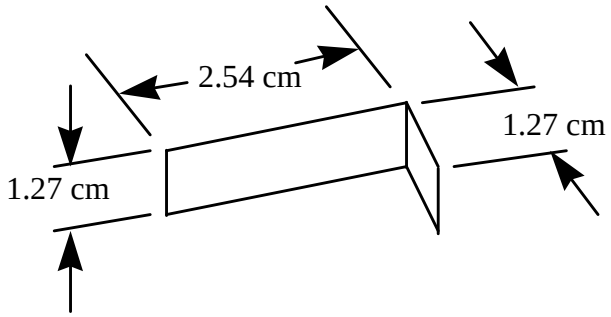

Figure 16. The dimensions and shape of the construction paper "crack" used in disc #8.

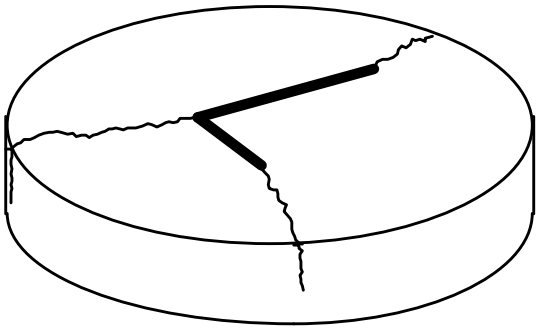

Figure 17. The resulting surface cracks in disc #8, shown with the bottom or "cracked" face up. The secondary cracks decreased in width as their vertical location increased.

A delamination was formed in disc #9 using a similar process. A 1.90 cm by 1.90 cm square was cut from construction paper. Roughly one half of the powder was poured into the mold and lightly packed with the die. The paper was placed in the center of the mold (Fig. 18), and the rest of the powder was added. The sample was die-pressed, CIP and fired. The paper within the disc burned away leaving a square shaped flat void parallel to the face in the center of the disc. This delamination was completely contained within the disc and did not reach the surface.

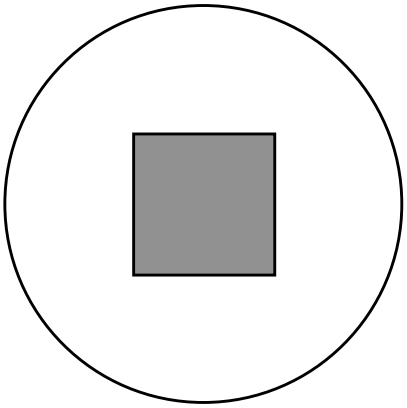

Figure 18. The location of the construction paper square “void” in disc #9.

Aluminum is often present in the manufacturing environment as well as steel, so disc #10 was created to test the effects of aluminum impurities in Zr-PBSN. Half of the powder was poured into the mold and lightly packed with the die. Aluminum filings were then poured onto the surface. They were concentrated in the center of the mold, but due to their small size (~ 0.1 mm) it was impossible to remove all of the shavings from the outer sections (Fig. 19). As a result there was a gradient in aluminum particle density that decreased as the distance from the center increased. The remaining powder was carefully poured on top and die-pressed. The sample was removed from the mold and inspected for damage. None was found so the disc was CIP and fired.

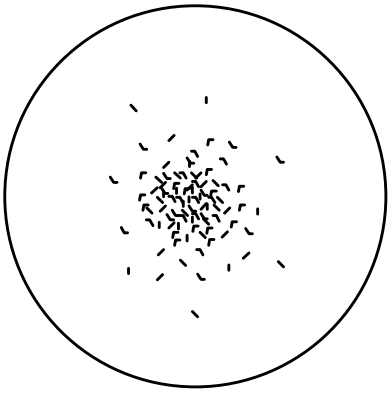

Figure 19. The schematic distribution of aluminum shavings in disc #10. The depth of the shavings is roughly one half the height of the disc.

Graphite powder was used to induce porosity in disc # 11. The graphite was very fine and mixed well with the ceramic powder. Graphite oxidizes to carbon dioxide at a temperature below 600°C so all of the volume occupied by graphite will turn into voids when the ceramic is fired. Roughly 1.5 g of graphite powder were added to the powder for one disc (~75 g) and sieved using a 500 micron screen to insure proper mixing. The powder was poured into a mold and die pressed. No damage was observed upon removal from the mold so the disc was CIP and fired. It should be noted that after removal from the mold the green ceramic material had a silver color to it, which was a result of the graphite. This new coloration was no longer present after firing, which indicated that the graphite had indeed burned away leaving only the Zr-PBSN material.

Samples which were 2.54 cm diameter discs with thickness' near one centimeter were prepared with induced porosity that was varied by two methods. Eight samples were made by die pressing at 133 MPa then CIP at pressures of 157, 210, 245, 280, 315, 350, 385 and 420 MPa. The varying CIP pressures should result in different packing densities, thus different porosities. Four samples were made by adding finely distributed graphite powder to the initial powder mix (Table III), die pressing at a pressure of 87.5 MPa and then CIP at 420 MPa. All samples were fired at 900°C for five hours. The graphite oxidized to carbon dioxide at a temperature much lower than this and was expected to result in pores.

Table III. The graphite and ceramic powder contents of samples G1-4.

Sample	Green Powder (g)	Graphite Powder(g)	% graphite by mass
G1	15.25	0.34	2.18
G2	14.40	0.35	2.37
G3	15.02	0.44	2.85
G4	14.40	0.50	3.35

The details of sample dome preparation can be found in the appendix. Due to the difficulty in preparing these domes the first priority was to obtain a good specimen with the radome geometry so no flaws were attempted in the first dome. Once a good radome shaped sample had been obtained, fabrication of specific defects, which endanger the successful completion of a radome, could then be attempted.

A crack located on the bottom that traveled vertically to height of 3 cm was observed after hand-sanding. After firing, there were five cracks that began at the base of the dome whose heights ranged from 1 to 3 cm. There was one surface crack that ran vertically that started at a height of 3 cm from the base and traveled up for approximately 6 cm. There were five surface cracks oriented horizontally (roughly parallel with the base) with an average length of 3 mm. There was one burst type defect located one third of the way from the tip, which had a diameter of 5 mm. These were the visible defects. All subsequent attempts to fabricate dome samples failed. The green dome either fell apart upon removal from the boot after CIP, which was generally the case for domes with intentional defects, or were damaged in the hand sanding phase of preparation.

Zr-PBSN disc-samples were constructed with fabricated flaws to simulate defects that could result in a radome manufacturing environment. Smaller discs were made with varying porosities by altering the CIP pressure or adding graphite powder to the green ceramic powder. Several small radomes were attempted, but only one survived. Although no flaws were purposefully fabricated in this particular dome, several occurred anyway. The reason for creating these samples was to evaluate candidate NDE method's ability to detect flaws of interest.

NDT METHOD EVALUATION

The samples constructed to simulate flaws in Zr-PBSN radomes were next used to evaluate candidate NDE methods as potential components in the radome NDE system. Methods such as transmitted light (in translucent radomes) and visual inspection, including alcohol wipes and other penetrants have been used in older generation radome inspection processes. Visible inspection is still a useful method, but it is limited in that it cannot detect internal defects such as porosity variation, internal cracks, voids and inclusions. Visual inspection is also dependent on the skill of the inspector. The goal of this project is to develop an automated system which can overcome these limitations. Candidate methods included transmission of infrared and visible light, thermal inspection and ultrasonic scanning.

TRANSMITTED LIGHT

Transmitted light methods were attempted using both visible and infrared wavelengths. A 100 watt light had been illuminated within the small dome, which had been shielded to prevent light leakage. The room was darkened and a charge coupled device (CCD) camera was used to test for visible light. Emission of light was not observed. A similar test was made with an infrared (IR) camera (Inframetrics 600). No transmission of infrared radiation was observed but variations in the surface temperature of the dome occurred due to the heating by the light. A final attempt to detect light transmission was made with a 10 miliwatt Helium-Neon laser (7.2 μm) as the source. Once again no transmitted light was observed. it was concluded that transmitted light is not a viable inspection method for Zr-PBSN radomes.

THERMAL ANALYSIS

The possibility of using the variations in external surface temperature, caused by heating the domes from within, to locate defects was investigated next. The emission characteristics of the Zr-PBSN material were observed to be constant across the surface when viewed at uniform room temperature, thus any variation in the emission spectrum was caused by surface temperature variation. Internal defects were detected by creating a temperature gradient across the thickness of the material and searching for perturbations in the heat flow. If some inconsistency within the material changed the overall heat conductivity across a section of the dome, the heat transfer from the high temperature area (inside) to the low temperature surface (external) would be altered and that surface would heat differently than flawless sections. It was the difference in infra-red emission due to varying temperature that the IR camera (Inframetrics 600) detected. Heat transfer was key to locating the imperfection, and an increase in heat flow resulted in a greater temperature difference on the surface and thus a greater contrast as shown by the camera.

When examining the sample discs heat transfer was maximized by first cooling the samples to 0°C in snow, which was conveniently located outside, and then heating one surface with a General Electric 250 watt Infrared_Heat[2] lamp. The camera was focused on the non-heated front surface, which had been dried, and variations in surface temperature were monitored as heat flowed from the back to the front surface. Attempts were also made to monitor the results when heat flowed in the opposite direction. The sample disc being observed was heated and then placed with one surface contacting packed snow and the other surface exposed to air. The exposed surface was monitored with the IR camera as heat flowed away from it. A greater temperature gradient could be established with this method, which resulted in a higher rate of heat flow and better defect detection.

Disc #8 was the first to be evaluated by IR inspection upon heating. Face “A” of disc eight had an exposed “L” shaped crack with smaller cracks radiating outwards from the corners of the “L”. Face “B” was smooth and featureless. Disc #8 was first cooled in snow and then allowed to heat to room temperature while face A was observed by IR. No sign of the crack was detectable on the IR image obtained. The disc was cooled again and this time face A was heated with the lamp while face B was observed by IR. The crack was still not visible. The disc was re-cooled again in snow and the procedure was repeated except that face B was heated while face A was observed. The resulting image is shown in Fig 20.

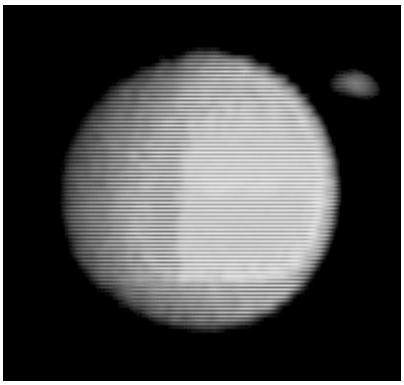

Figure 20. An IR image obtained by first cooling disc #8 in snow and then heating the un-cracked face. The presence of an “L” shaped crack is just detectable in the image of the cracked face.

The “L” shaped crack was visible in this image, but the secondary cracks were not. An attempt to get better definition was made by cooling the disc, then heating face A with the lamp for 30 seconds. The lamp was removed and face A was observed with the IR camera. A faint “shadow” could be seen which indicated the presence of the main crack, but the secondary cracks were not visible. This test was repeated with face B, but the image of the crack was not detectable on the smooth surface. These results indicated that IR imagery was not a viable method for detection of radial cracks since it did not show the secondary cracks, which were easily visible to the naked eye.

Disc #9 contained the square delamination in the center of the disc, oriented parallel to the flat faces. Cooling the disc and then heating one face as done with disc eight, did not show the delamination. An attempt to increase the heat flow from the hot to the cold face was made by placing one face in the snow and heating the other face with the lamp. The image shown in Fig. 21 was obtained by removing the disc from the heat and snow and then immediately observing the heated face with the IR camera. In this image the lighter areas are the hottest, and the light region in the center represented the square delamination, which hindered the heat flow away from the hot face. It was difficult to tell if this was caused by the delamination or edge effects, but this contrast quickly disappeared after the disc was removed from the heating-cooling environment. Image processing techniques were used in an attempt to clarify the image, but the results were inconclusive.

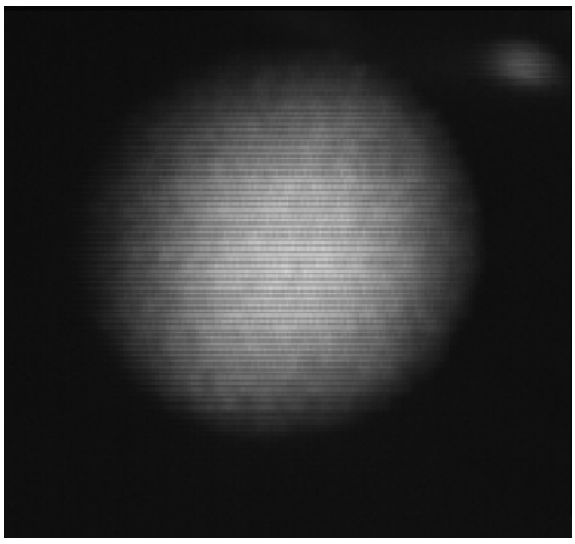

Figure 21. An IR image of Disc #9 obtained by observing the heated face directly after removal from the heat-cold environment. The light area in the center was a hotter region that was caused by the delamination hindering the heat flow away from the hot face.

Disc #11 was constructed to have uniformly high porosity. To test the effects of porosity on heat transfer and IR imaging disc #11 and disc #2, a disc that was defect free were

both cooled in snow and then placed on a warm surface (35 °C). After two minutes the unheated surfaces of the discs were observed with the IR camera (Fig. 22). Disc eleven was noticeably cooler than the disc with less porosity. The increase in void content resulted in a decrease in heat transfer, which was expected since the gas in the voids, had a much lower heat conductivity than Zr-PBSN.

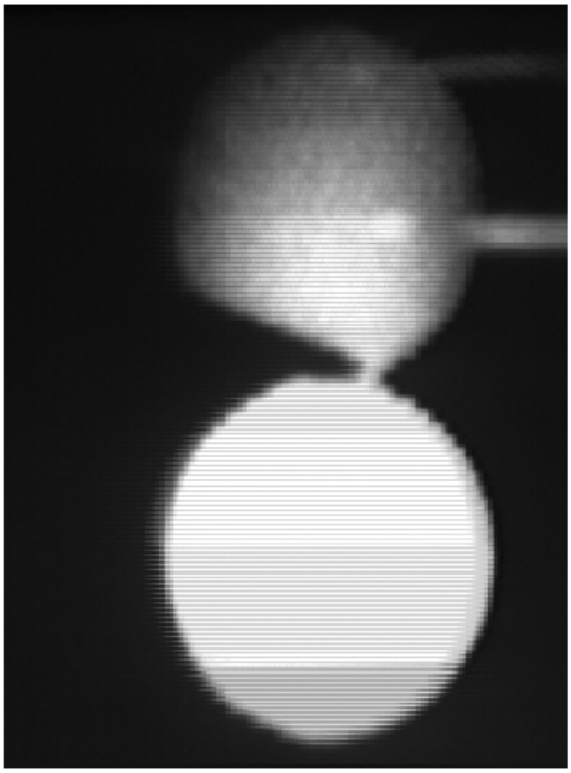

Figure 22. Disc #2 (on the top) is normal with no defects, while disc #11 (below) was fabricated to have a uniformly high porosity. The discs were cooled and then placed on a warm surface. The image is of the unheated face. The lighter or cooler coloration on disc eleven indicates a lower surface temperature caused by a decreased heat conductivity.

Disc #4, which was constructed to have a region of high porosity near the center of the disc was placed in hot tap water (40°C) to heat the sample evenly and avoid any "point" heating, or heating one point of the disc face more than the others, which may have occurred with the heat lamp. One face was placed in the snow and the exposed face was

observed with the IR camera. The image obtained is shown in Fig. 23. The dark, or colder region slightly off-center corresponds to the location of the high porosity region. The disc was exposed to the snow for forty five seconds and then the cool face was dried and observed (Fig. 24). The image showed the cooler region more distinctly in the same off-center location. It is unclear why the high porosity region is cooler on both the heated and cooled face, but the location agreed with results obtained by ultrasonic inspection.

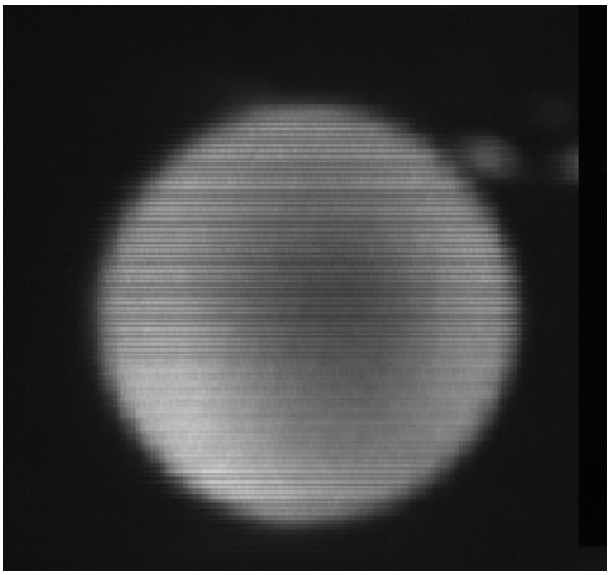

Figure 23. The image of disc four which has been uniformly heated in water and then cooled from the bottom by snow. The dark or cooler region just off-center represents the area of high porosity.

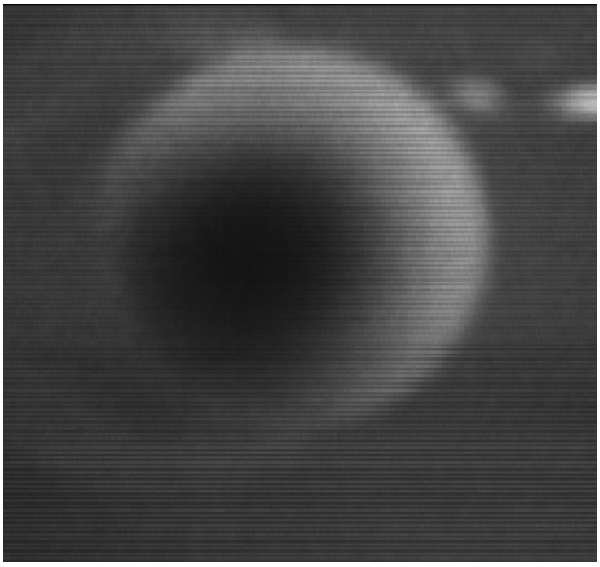

Figure 24. This image shows the cooled face of disc four. The high porosity area is shown as the dark region near the center of the disc.

No images were recorded of disc #5 due to destruction of the sample. The disc contained a large delamination that went through most of the disc. The disc was heated in water and then one face was placed in snow. Initial images showed the region that was not delaminated cooled the fastest, but due to mechanical and thermal shock, the delamination propagated all of the way through the sample which split in two before images of the disc were recorded. The voids were not detected by IR inspection, but were clearly visible in the newly exposed faces of the disc. To avoid similar failures, no attempts were made to detect the steel shavings in the partially delaminated disc #7.

Disc #10 had aluminum shavings in the center. The disc was heated in hot water and then one face was placed in the snow. The exposed face was observed with the IR camera (Fig. 25). The images show that the edges cool faster than the center. It was thought that the center should cool faster due to aluminum's higher heat conductivity, but this was not the case. One explanation was that this was caused by edge effects, or higher cooling rates around the edges, but later analysis with ultrasonic methods showed that there was a delamination on the center of the disc which would explain why the heat

flow was reduced in the center of the disc thus resulting in slower cooling compared to the edges.

The small dome was packed with snow and cooled. A stand was constructed to support a soldering iron so that it could be used to heat the dome from within (see Fig. 26 a). The heating set-up did not heat the dome uniformly, but by adjusting the temperature window of the IR equipment, the region of interest can be viewed. The burst type defect is easily visible as a cool area when heated from within (Fig. 26 b). Many surface cracks that were easily visible to the eye were not visible with the IR system. A previously unobserved internal flaw was identified in the bottom third of the dome. It was not positively characterized, but it was thought to be a region of high porosity or a delamination, based on the way it hindered heat flow.

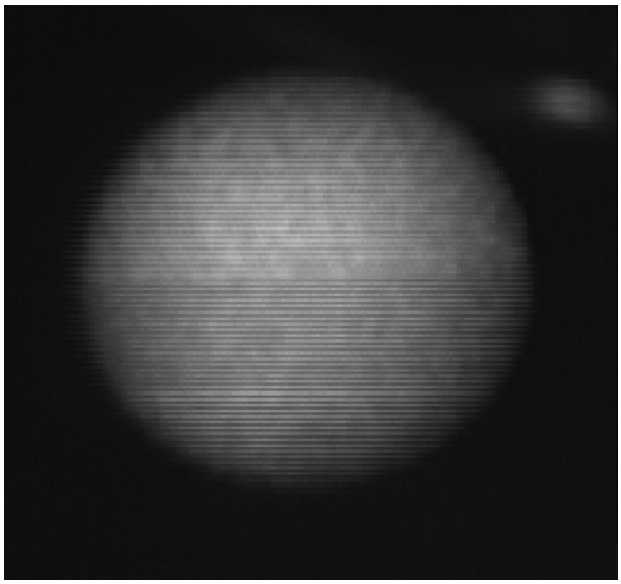

Figure 25. An IR image of the hot face of disc # 10, which contained a delamination in the center, caused by the addition of aluminum shavings. The cooler or darker area around the edges indicates a greater heat flow away from the hot face to the cool face.

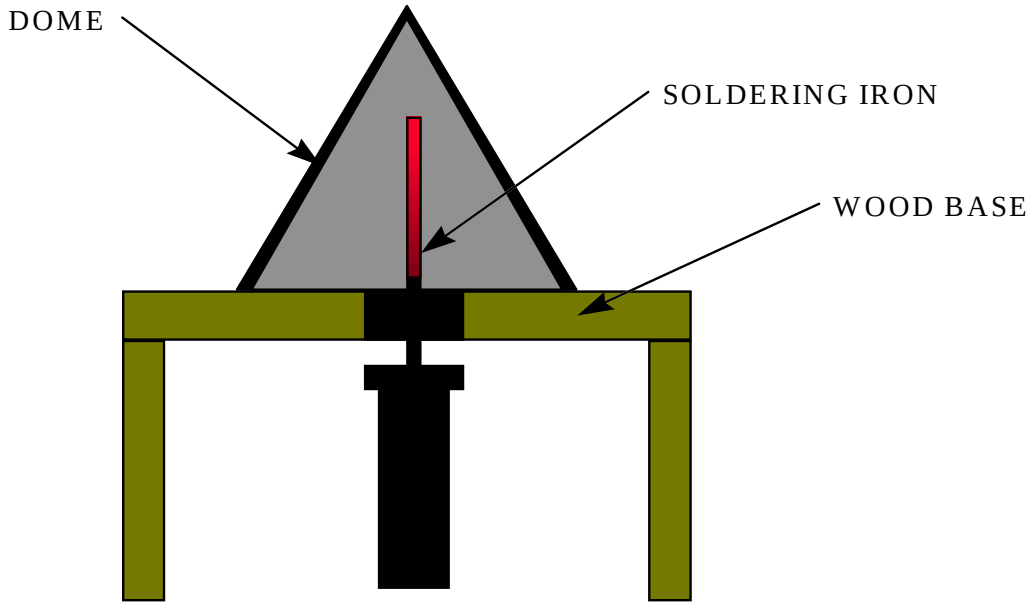

(a)

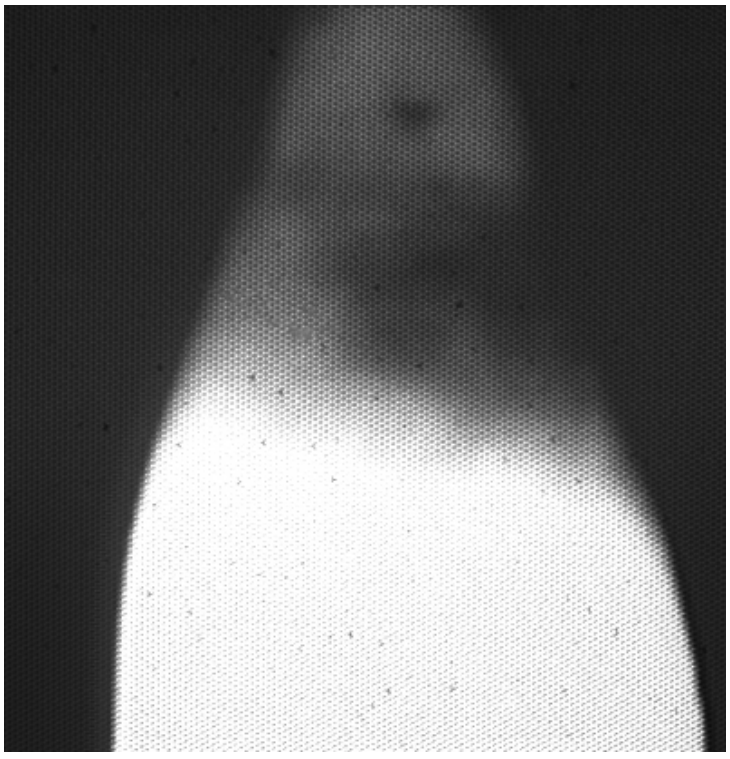

(b)

Figure 26. (a) The heating setup for viewing the small domes with IR. (b) An IR image of the small dome, which has been cooled and then heated from within. The burst type defect is visible as the small, dark, circular region near the top of the image.

IR imaging does not show all defects well enough to be considered for this project. Cracks that are oriented parallel to the direction of heat flow do not show up well. Small radial cracks that were easily visible to the eye were not present on IR images. Defects that are small compared to their depth within the material are also difficult to image by this method. For these reasons, IR imaging was eliminated as a candidate NDE method.

ULTRASONIC C-SCAN

The mechanical properties of Zr-PBSN make it well suited for ultrasonic inspection. The material has a very high modulus and transmits sound energy with little attenuation. It is non-crystalline and thus isotropic, which means the wave velocity is independent of direction within the material. It can be immersed in water with no long-term effects. It should be noted that this material is porous and will absorb water if left submerged for a long period of time (over three hours), but will lose this water if heated. The pores reduce the modulus of the material and thus reduce the velocity of sound in Zr-PBSN, but it was observed that no significant attenuation of compressive wave energy occurred. When pores absorbed water the compressive wave speed in Zr-PBSN increased due to the incompressibility of the water trapped in the pores.

Ultrasonic inspection involves injecting an elastic wave into the part at a certain location and then detecting that wave after it has passed through the area of interest. Information about the material through which the wave has passed can be obtained by examining the collected wave's intensity and time of flight. A major limitation of inspection by ultrasonic techniques is that the feasibility is very dependent on the geometry of the part being inspected. Elastic waves will reflect and refract at material interfaces according to

Snell's law. The two conditions that affect the extent of reflection and refraction are the angle of incidence of the wave and the difference in wave velocity between the two materials. The ideal component geometry has two surfaces that are parallel to each other. A wave will not change direction as it goes from one material to another if the angle of incidence is zero degrees. This situation is desirable because a wave can be generated and collected by a single transducer (Fig. 27) using the pulse echo configuration.

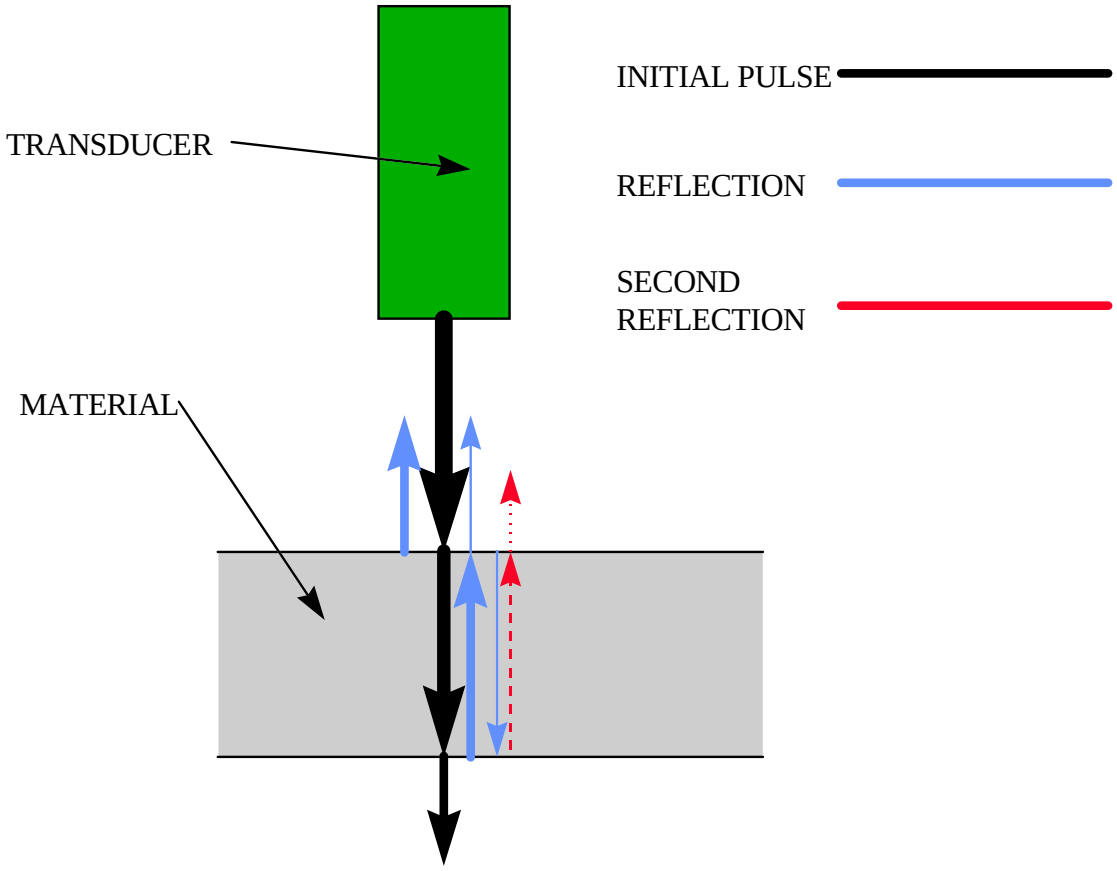

Figure 27. The pulse-echo configuration in which the wave is generated and detected by the same transducer. This configuration is limited by the component's geometry.

The dome geometry consists of a thin-walled cone, which has some curvature, and a constant wall thickness. This geometry is not the simplest case, but if a way can be found to keep the transducer, and thus the injected wave perpendicular to the surface of the radome then the reflected wave will return back to the transducer because the inner

and outer surfaces are parallel. This is a mechanical problem that can be overcome with a properly designed scanning fixture. The question that remains is whether ultrasonic inspection can detect the flaws of interest in Zr-PBSN. The inspection method of interest is ultrasonic C-scanning which involves injecting a wave into the material and monitoring the intensity of the back-wall reflection. The intensity is given a numerical value and recorded for that particular location. The transducer is moved and the process is repeated until the entire area of interest has been inspected. The data is plotted in two dimensions with a color or gray-scale used to represent different intensity values. A defect will affect the intensity of a wave that has passed through it and this is usually reflected in the resulting C-scan. The discs were inspected by C-scanning to test this methods ability to find defects of interest.

Initial scans were done using through-transmission. This involves using a transducer to generate the a wave, which travels through the material and out the other side, where it is detected by a second transducer, which in this case was a pinducer or very small transducer. Through transmission showed promise as an inspection method for this material, but complications arose due to the radome geometry. The second or detecting transducer would be very hard to position within the dome.

The pulse-echo technique involves using a single transducer to generate a wave, which travels into the material and then reflects back, usually from the back surface, through the material to the transducer, and the intensity of this reflected wave is monitored. This setup would work with the dome geometry, because the transducer could easily be positioned from outside the dome. The main concern would be to find a way to keep the transducer perpendicular to the surface. This setup was also tested on the sample discs to see if the defects which were present in the discs could be detected. A 15 MHz, 0.25" diameter, 1.5" focal length transducer was used because it offered a good combination of power and resolution.

Scanning was first tried on disc #8, which contained the “L” shaped surface crack. The disc was oriented so that the crack was on the bottom face and the top face was flaw free. The wave was injected from the top, traveled through to the back surface, was partially reflected, exited the top surface and was detected by the transducer. The first scan (Fig. 28) was done by monitoring the intensity of the back wall reflection. The location of the main and secondary cracks are clearly evident as regions of low intensity. The intensity loss was caused by the crack scattering the wave away from the transducer, decreasing the observed intensity.

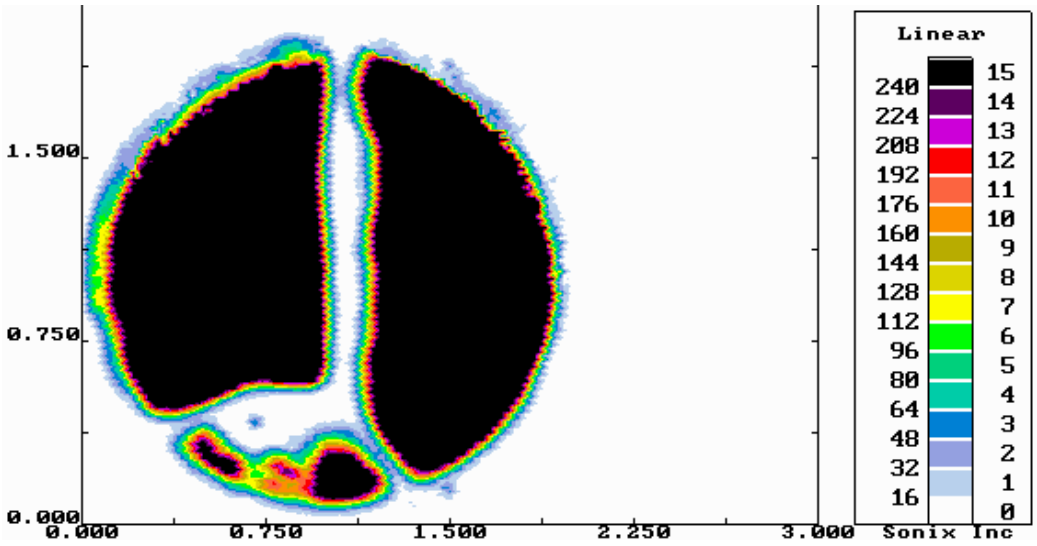

Figure 28. A C-scan of disc #8, containing an “L” shape crack with smaller secondary cracks radiating from the corners of the “L”. This scan was made by monitoring the back wall reflection in a pulse-echo setup.

A second scan was made by monitoring or gating the reflection from the crack. The manufactured crack had a fairly uniform depth, which produced a strong reflection (Fig. 29). The secondary cracks are also evident, but not as well defined.

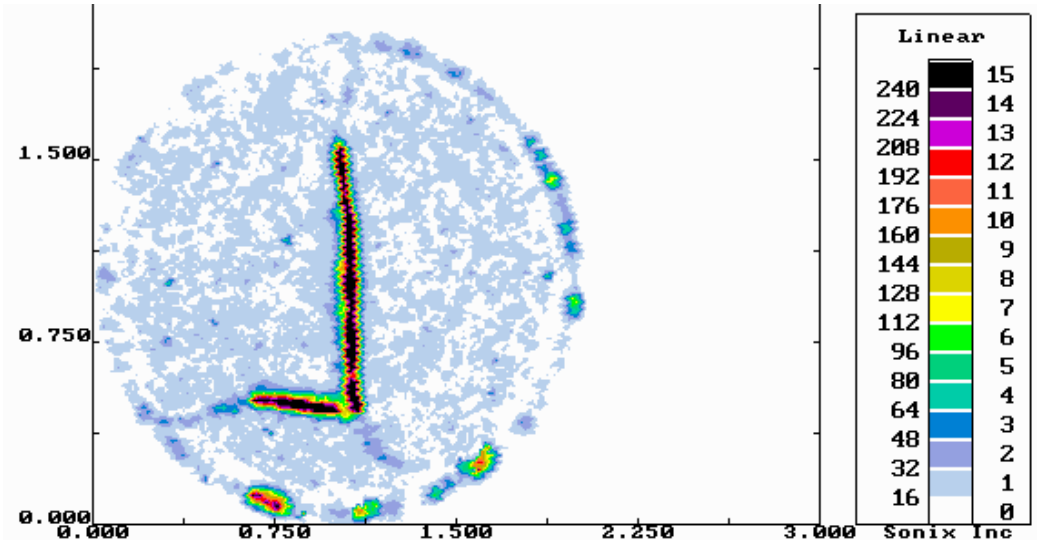

Figure 29. A scan of disc #8, which was made by gating the reflection from the crack in pulse-echo mode.

Disc #9 had a square piece of paper pressed into its center so that a delamination would form. Fig. 30 is a scan that was made by gating the sound reflected from the delamination. The fabricated delamination is evident as well as a secondary delamination, caused by the presence of the paper upon release from the mold. The secondary delamination had a lower intensity reflection due to the random crack surface, unlike the fabricated delamination which has a smooth, uniform surface. A scan was made by gating the back wall reflection (Fig. 31). This image was harder to explain than most of the other images. The image contains a thin ring that appears to be the outer portion of the disc as well as a square shape in the center that is obviously the result of the fabricated delamination. The square image is actually the second reflection from the delamination. The delamination is in the center of the disc. The incoming wave is reflected from the delamination and travels to the top surface. Some of this wave passes through to the water, while the rest is reflected back into the disc. This wave travels back to the delamination where it was reflected a second time back to the surface. This second reflection has traveled the same distance as the first back wall reflection and

arrives at the detecting transducer at the same time. Reflections are monitored by their time of flight (TOF), which is why a scan of the back wall reflection also shows the second reflection of the delamination located in the center of the disc. The secondary delamination does not show up because the reflection from the non-uniform surface was not as strong as the reflection from the primary delamination and no longer intense enough to be detected.

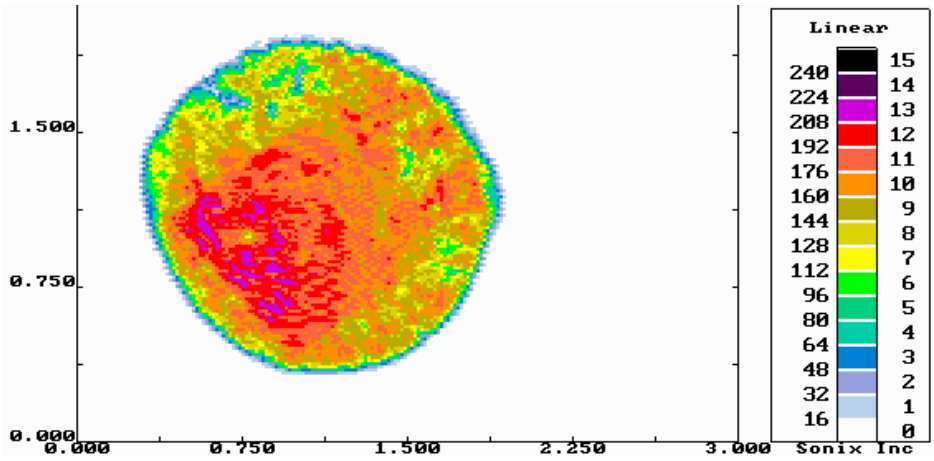

Figure 30. A scan of disc #9 made by gating the first reflection from the delamination.

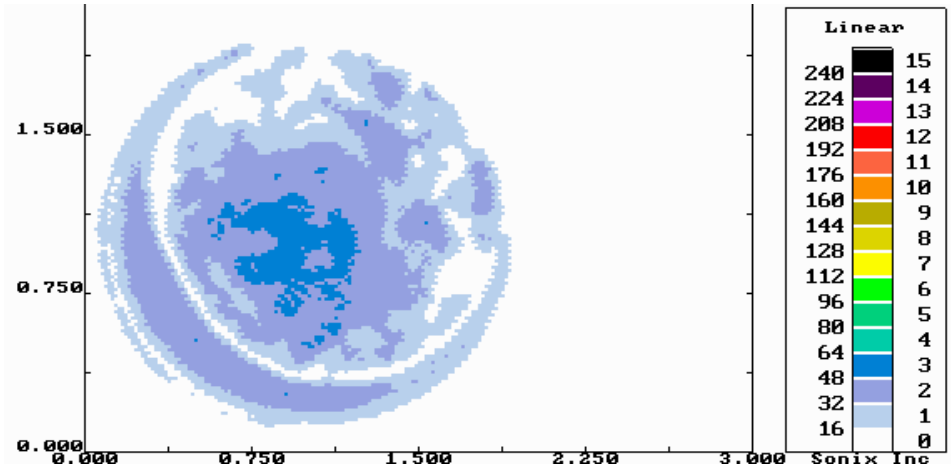

Figure 31. A scan made by gating the back wall reflection of disc #9. The second reflection from the delamination located in the center of the disc also was recorded because it had the same TOF as the first back wall reflection.

Disc #10 contained a thin layer of aluminum filings in a flat circular shape located in the middle of the disc. The presence of the filings caused an internal delamination, which can be seen in Fig. 32, to form upon removal from the mold. Fig. 32 is gated upon the reflection from the aluminum and shows a high intensity reflection from the aluminum as well as a less intense reflection from the delaminated area. The delamination is not located evenly around the aluminum, but exists primarily to one side (the top of the image).

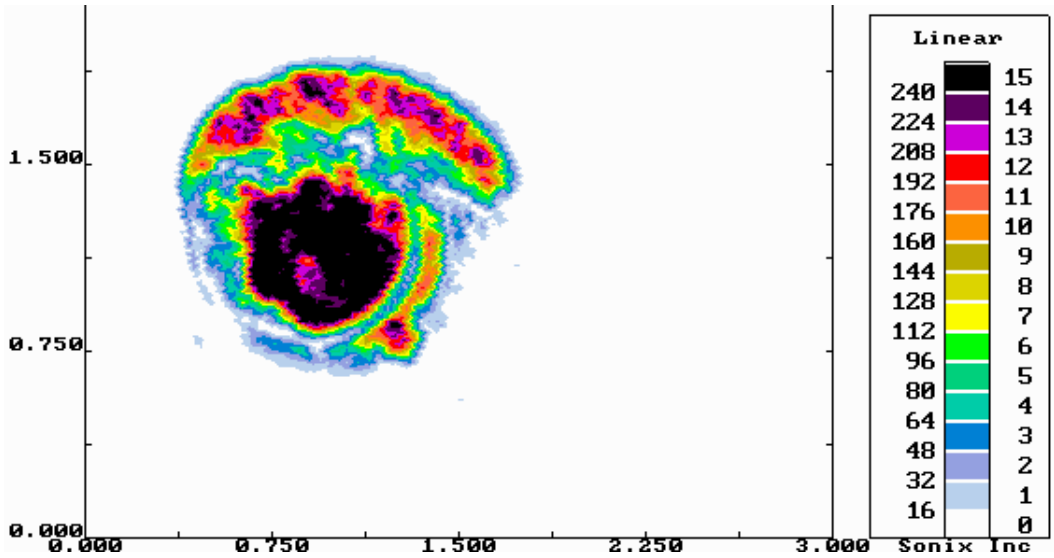

Figure 32. The image obtained by gating the reflection from the aluminum filings and secondary delamination found in disc #10. The secondary delamination does not reflect the wave as well as the aluminum, and was less intense.

When a scan was made by gating upon the back wall reflection (Fig. 33) the secondary delamination was clearly shown by its lack of reflection. The aluminum's second reflection, which arrives at the transducer at the same time as the first back wall reflection was intense enough to be detected by the transducer.

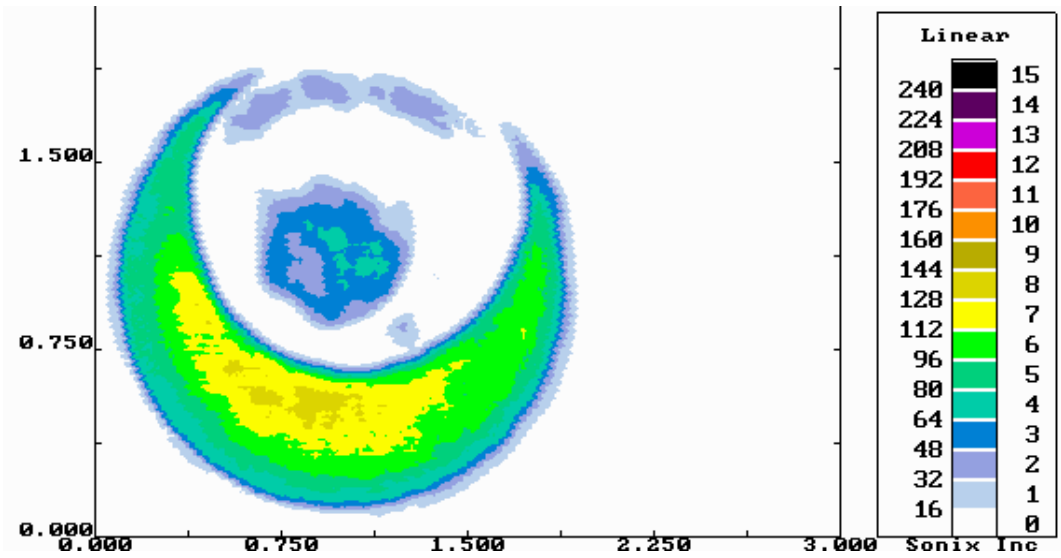

Figure 33. A C-scan of the back wall reflection of disc #10. The secondary delamination scatters this wave and shows as the white, circular region contained within the disc. The second reflection from the aluminum also register in this image because it has the same TOF as the primary back wall reflection.

Disc #4 had a zone of high porosity in its center. Fig. 34 is an c-scan made from the back wall reflection. The region of high porosity is clearly visible as the circular, low intensity region located just off-center.

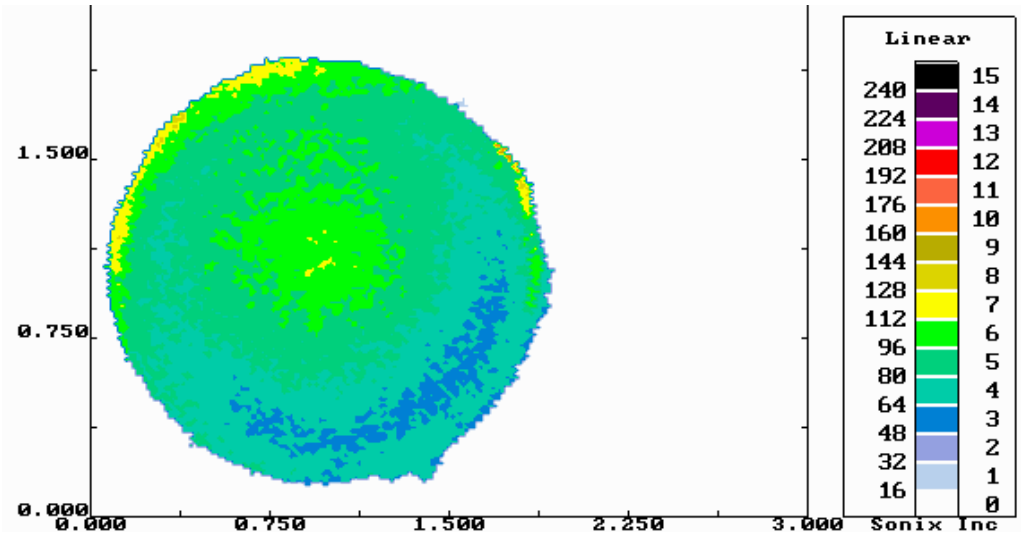

Figure 34. A C-scan of the back wall reflection of disc #4. The region of high porosity is shown as the circular, area of lower intensity located slightly off-center.

Disc #5 contained six triangular shaped voids located in a circle in the center of the disc. The disc partially delaminated upon removal from the mold, but was fired anyway. The delamination propagated completely through the disc during infrared testing due to mechanical and thermal shock. In the newly exposed face the six voids were clearly visible. Fig. 35 was obtained by gating on the reflection of the voids. Five of the voids showed clearly, while the one located in the upper right of the circle was only partially shown. Some reflections from the delamination surface were also visible in the lower right.

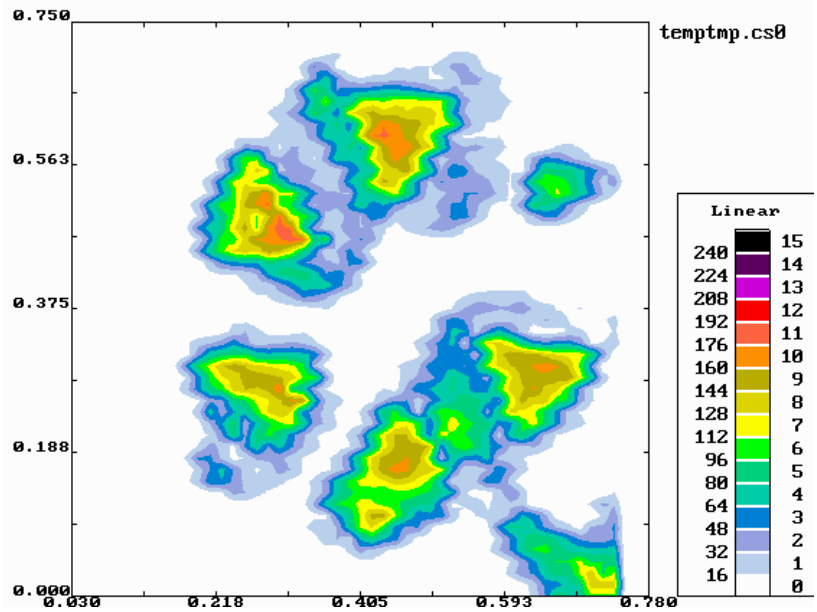

Figure 35. A C-scan of the reflections from the voids created in disc five. Five of the triangular voids were clearly visible in a circular pattern, while the sixth void, located in the upper right corner of the circle, was only partially shown.

Attempts were made to C-scan the small dome ultrasonically but the results were unsatisfactory. Surface cracks located near the base were not clearly shown and the subsurface flaw located by the IR camera was not detected. This was most likely due to the very inconsistent nature of the Zr-PBSN which resulted from hand processing. The variation in packing density caused adverse affects on wave propagation which rendered

the resulting C-scans meaningless. A full size dome obtained from Loral, was inspected. The equipment was unable to scan the dome due to its size and shape, but inspection of the wave form obtained by hand positioning indicates that pulse-echo ultrasonic c-scanning is a viable method for this geometry.

Ultrasonic inspection by C-scan with the pulse-echo method of wave detection has shown that it can detect flaws of interest in flat disc shaped samples. Its failure to image defects in the small dome was due to gross inconsistencies in the dome material, and not the geometry of the specimen. This method can be run with little operator involvement once the initial setup has been completed, but a skilled operator is needed to properly interpret the resulting scans. Regions of interest, found with the initial scan can be closer examined with a local high-resolution scan. A method to characterize local porosity via ultrasonic methods in Zr-PBSN has been developed.

DETERMINATION OF POROSITY

In applications where performance engineering is involved, the porosity is extremely important due to its effect on dielectric and mechanical properties. Porosity can be characterized in phosphate-bonded silicon nitride by correlating the velocity of a compressive elastic wave in this material to a porosity value. The wave can be generated and detected with the ultrasonic transducer and computer used in C-scanning. This method allows for the determination of porosity in a small volume of the sample and can be used to quantify porosity variations in a component unlike bulk methods such as the Archimedes method which gives an average value for the entire component.

Sample discs were constructed to have varying porosities by addition of graphite powder to the initial ceramic powder and by reduction of CIP pressure. The porosity of each

sample was characterized by the Archimedes method following the guidelines form ASTM designation C 373 - 88, Standard Test Method for Water Absorption, Bulk Density, Apparent Porosity, and Apparent Specific Gravity of Fired Whiteware Products. The porosity for each sample was measured four times to account for human error.

The sample was dried in a furnace overnight at 150 C. The velocity of a longitudinal elastic wave was then determined for each sample. The sample was placed in water then tested immediately using a Panametrics 15 MHz, 0.25" diameter, 1.5" focal length immersion type transducer to generate a longitudinal pulse which traveled through the water and struck the flat face of the sample with a 0° angle of incidence. The wave was reflected off of both the front and back surfaces of the sample. The reflected waves traveled back to the transducer which converted the mechanical energy of the reflections into electrical signals, which where displayed with a 100 MHz oscilloscope.

The time difference in the arrival of the front and back surface reflections at the transducer represented the amount of time it took the wave(longitudinal) to travel twice through the thickness of the material. The velocity of the wave as it traveled through the material can be determined by formula (1)

$$V = 2*d/t \qquad (1)$$

where V is the velocity of the wave, d is the sample thickness and t is the arrival time between the front and back reflections.

The results in Fig. 36 show the average porosity for each sample with the standard deviation represented by the error bars. The four samples prepared by the addition of

graphite powder had higher porosities(20% - 23%) than those samples made by varying the CIP pressure(16% - 18%).

Ultrasonic evaluation of a material involves injecting an elastic wave into a component. The wave propagates through the material and is then detected. The detected wave reflects the global effect of all the material through which it passes. The pores in phosphate-bonded silicon nitride are very small, numerous and well distributed which is a situation that is well suited to evaluation by ultrasonic means. If a frequency of 15 MHz is used and a velocity of 3000 m/s is assumed then the wavelength is 0.2 mm. The microscopic pores do not interact directly with a passing wave, which would result in significant scattering and attenuation, but do affect the material's modulus, which will affect the wave velocity.

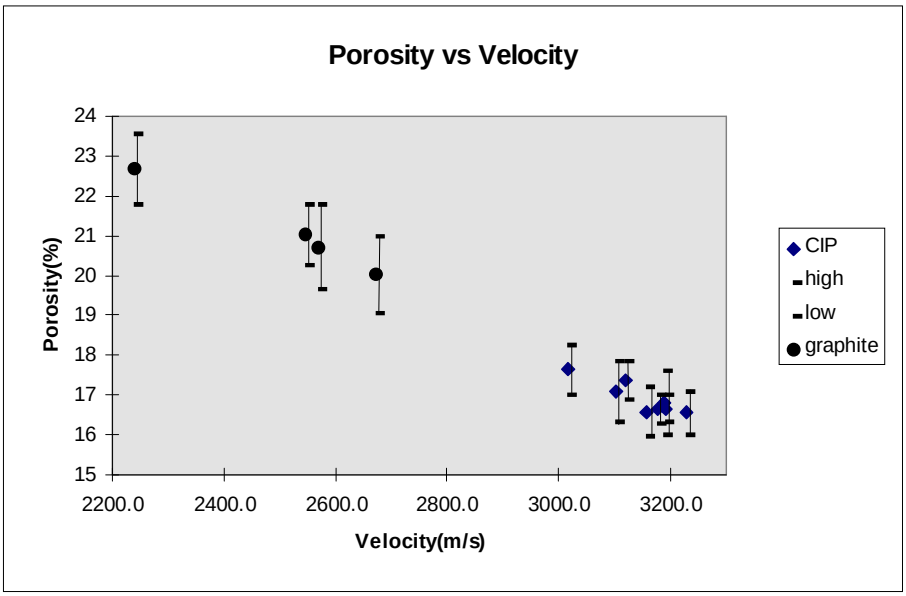

Figure 36. A graph of porosity as a function of velocity. The round markers represent the samples prepared by adding graphite powder, while the diamond markers represent the samples prepared by varying the CIP pressure.

Early attempts to characterize porosity dealt with the stress strain relationship and its dependence on porosity. Empirical and theoretical relationships were obtained

[7,8,9,10,11,12]. The velocity of sound in an elastic solid is directly related to the square root of the modulus of that material, and this relationship was often used to test the various models.

Wang developed a theoretical model [13] by assuming that the sintering process consisted of an array of closely packed spheres (simple cubic for simplicity) that initially contact neighboring spheres at six points, but as densification increased the points turned into circular faces that grew in area until complete densification or zero porosity occurred. Wang described the degree of densification by a contact angle, θ, which is defined as the angle whose vertex is at the center of the sphere and whose endpoints lie diametrically opposed on the circle created by the interface with an adjoining sphere, thus θ increased as the diameter of the contact face increased. The transition point from open to closed porosity occurs when $\theta = 45°$ and complete densification occurs when $\theta = 54.74°$. This geometric treatment of densification results in a model that is inherently capable of treating the transition from open to closed porosity. A correction factor was included to account for non-ideal alignment of the matrix, which does not affect porosity, but does affect the elastic moduli. The resultant model is of the form

$$E(P) = E_0 \exp[-(bP + cP^2)] \qquad (2)$$

E(P) = elastic modulus of porous isotropic material
E_0 = elastic modulus of non-porous material
P = percent porosity/100
b, c = empirical material parameters.

It should be noted that for this model, the elastic modulus is controlled by the degree of densification and is independent of the particle size. The number of pores was assumed constant, while the size of the pores increases with increasing porosity. Velocity was

directly substituted for modulus into equation (2) and a regression was performed to determine the values of the material constants that correlated best with the observed data. The results can be seen in Table IV.

Kupkova [14] approached the problem differently. A relationship for the elastic modulus and porosity was obtained by first modeling the effects of porosity on the velocity of sound and then finding the elastic modulus from the predicted sound velocity. His first step was to develop a dispersion relationship that was a function of porosity as well as the wave number (k). For small values of k the dispersion relationship for a uniform material is

$$\omega = c_i * k \qquad (3)$$

ω = frequency
c_i = velocity of mode i
k = wave number.

The wave number, k, was limited to small values(long wavelength approximation). This assumption allowed the motion of the center of mass of each elementary cell to be considered instead of each atom within that cell. The power with which one elementary cell, when it was disturbed from equilibrium position, acted upon another was modeled. The effect of each pore on this system was then accounted for by considering the mass removed by the volume of each pore and adding this effect to the model. Each pore was considered to have uniform size and shape as well as being uncorrelated with any other pore (closed porosity). The porosity was increased by adding pores of the same size. The wavelength was considered to be much larger than the pores and the polarization of the wave was assumed to be unchanged by the pores. The resulting dispersion and velocity relationships for a porous material were

$$\omega = \left[\frac{1+a_i P}{1-P}\right]^{1/2} c_i(0)k \tag{4}$$

$$c_i(P) = \left[\frac{1+a_i P}{1-P}\right]^{1/2} c_i(0) \tag{5}$$

a_i = pore shape factor for mode i

$c_i(x)$ = velocity of mode i at percent porosity = x.

The parameter a_i depended on the shape and size of the pores, but not the number. A regression showed that the observed data correlates to the parametric values shown in Table IV. The average deviation listed in Table II was a measure of how closely the observed data correlated to the predicted data. A graph comparing the two models and the observed data is shown in Fig. 37.

It was apparent that for this range of porosity it was unclear which model best describes the porosity-velocity relationship. It is unlikely, however, that materials with porosities outside of this range will be produced by the current processing techniques and either model was acceptable for this application.

It was possible to determine the porosity of phosphate-bonded silicon nitride by measuring the velocity of a longitudinal elastic wave that had traveled through the material. Models from Wang and Kupkova have been applied with similar results over the small range of achievable porosities. Due to the divergence of the two models, the porosity must be within the range tested (16-23%) for the models to be accurate. This is not a serious limitation as it is unlikely that porosities outside of this range can be obtained with the current manufacturing techniques. This measurement allowed for

Table IV. Parameters for the Wang and Kupkova models.

Model	C_0	a_i	b	c	average deviation
Wang	5223		2.078	23.02	0.151
Kupkova	4591	-3.610			0.182

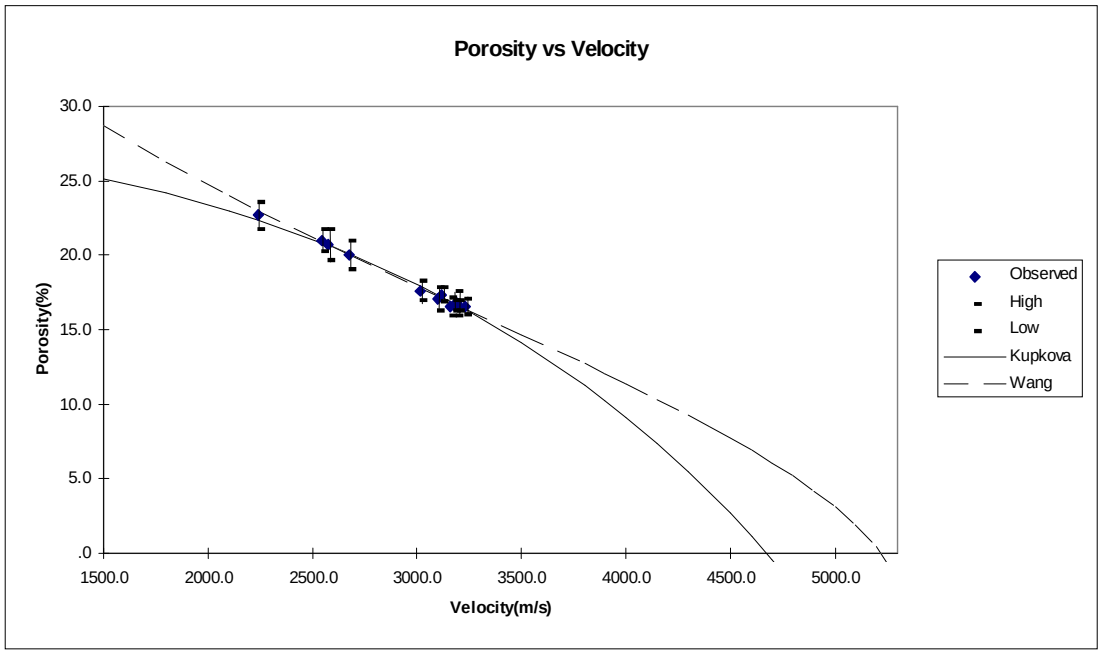

Figure 37. A graph comparing the models by Wang and Kupkova with the observed data.

increased characterization in radome evaluation, which had significant importance because small variations from expected porosity could endanger the functionality of the radome.

PROPOSED SCANNING SYSTEM

The radome NDE system must accommodate several design and functionality constraints. It must be capable of inspecting a range of dome sizes and shapes and it must detect any flaw that could affect the functionality of the radome. A system that minimized operator involvement as well as the length of time necessary to complete an inspection would be desirable. The output of the inspection should clearly show any defects in such manner so that their position on the dome was easily located. Larger domes are heavy and awkward for a single person to lift. The apparatus should be designed so that a single operator can load and unload a dome with little risk to either operator or dome. With these considerations in mind, a system has been designed and is under construction.

The method of NDE that has been chosen is ultrasonic inspection with a pulse-echo detection configuration. Ultrasonic inspection has shown that it can detect defects such as cracks, delaminations, porosity variation, and impurities in Zr-PBSN material. It was felt that this method could detect any possible flaw that compromised the functionality of a radome.

This evaluation method involves scanning, or making evaluations over the entire surface of the dome and mapping the results. Each evaluation represents the condition of that portion of the radome from which it was made. For full sized radomes, initial scans will be done at a step size of 0.01”. The output of each evaluation will be a value representing the intensity of the detected ultrasonic wave. The data will be displayed in the same format as an ultrasonic C-scan, by using a color palette to represent the intensity value, and the location in X-Y space representing a location on the radome surface. The analog reflection signals will be converted into digital intensity values which can be displayed, saved, and manipulated by computer.

There are several methods for detecting the signal which is representative of the dome's condition. Due to geometrical constraints it has been decided to use the same instrument as the source and detector of this signal. This type of scanning requires that the source/detector, which is a transducer for ultrasonic inspection, be kept perpendicular to the surface while scanning. The radome's non linear outline complicates this, but the radome is axially symmetric. This shape lends itself to rotational scanning. A turntable could be used to rotate the dome while the scanning unit stepped in the axial direction as shown in Fig. 38. Different turntable bases could be manufactured for different sized domes and the scanning unit could mechanically track along the surface so that various dome shapes could be accommodated. The entire assembly would sit in a tank that held water, which would act as the couplant for ultrasonic inspection. The problem with this set up is that loading and unloading a radome would be very awkward and would put the radome at risk.

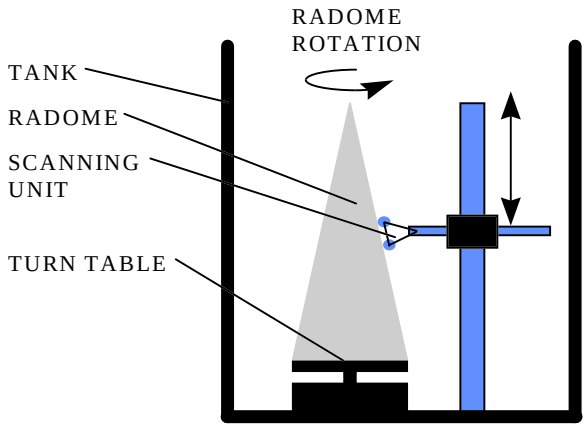

Figure 38. A diagram of the turntable set up. The dome sits on the turntable, which has exchangeable bases to accommodate different size domes. The scanning unit steps vertically and mechanically follows the contour of the dome so that the signal source/detector is always perpendicular to the surface of the dome. The entire system would sit in a tank of water.

Another means of rotating the radome would be to lay it on its side and support it with rollers. One roller could be used as a drive wheel and the others would rotate freely. The scanning unit would be overhead, step horizontally and follow the contour of the dome mechanically. Changing the roller positions could allow for the scanning of different size radomes. Fig. 39 is a diagram of the proposed set up. This design eliminates the loading, unloading problem while still taking advantage of rotational scanning.

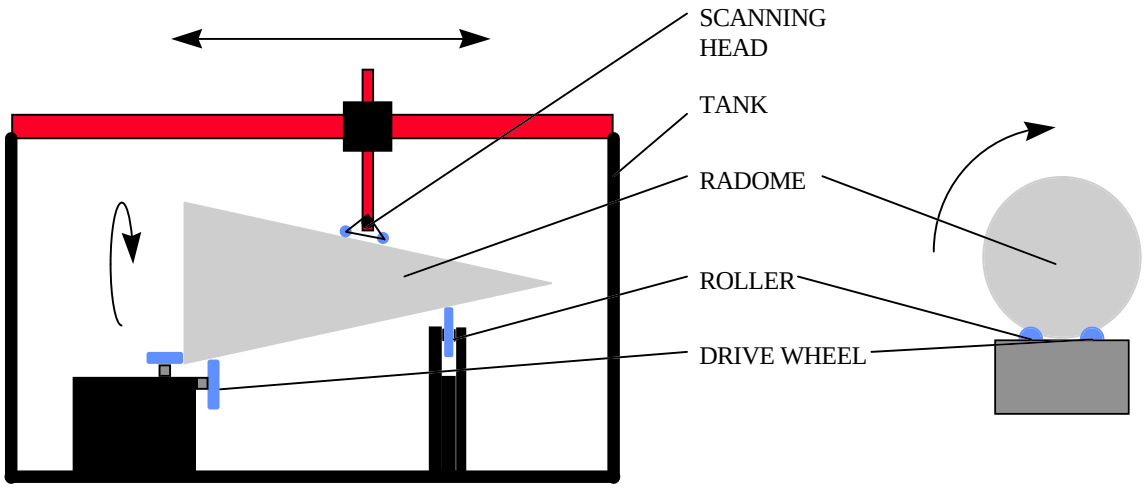

Figure 39. A diagram of the horizontal cradle scanning set up. The dome sits upon rollers, which make up the cradle. The scanning unit drops down from above to mechanically follow the contour of the dome as it steps axially.

The cradle consists of six rubber support wheels used as rollers. Four are mounted vertically and two are mounted horizontally. They operate in pairs to position and rotate the dome. The two vertically mounted pairs support the dome at the base and tip. The pair at the tip can be moved closer or further from the base pair to accommodate different size radomes. One of the rollers in the rear pair will be used as the drive wheel, which will be mechanically linked to a computer controlled stepper-motor. The pair of horizontally mounted rollers will support the bottom of the radome and with the help of gravity, maintain the radome's horizontal position.

The scanning unit will be supported by a rail-table mounted over the cradle. This will step axially via a computer controlled stepper-motor. A linear bearing mounted on the rail-table will be used to horizontally support a shaft that can move freely in the vertical axis. The scanning unit, which will be attached to this shaft, pivots and uses rollers to follow the contour of the radome, thus correctly orienting the scanning unit to the surface of the radome. A detailed diagram of the scanning unit is shown in Fig. 40. The scanning unit will follow the contour of the dome with alumina bearings which roll across the surface. The transducer will be attached to the scanning unit with interchangeable plates that when mounted to the scanning unit, will correctly position the sensor for that particular application. This will allow other types of scanning to be accommodated.

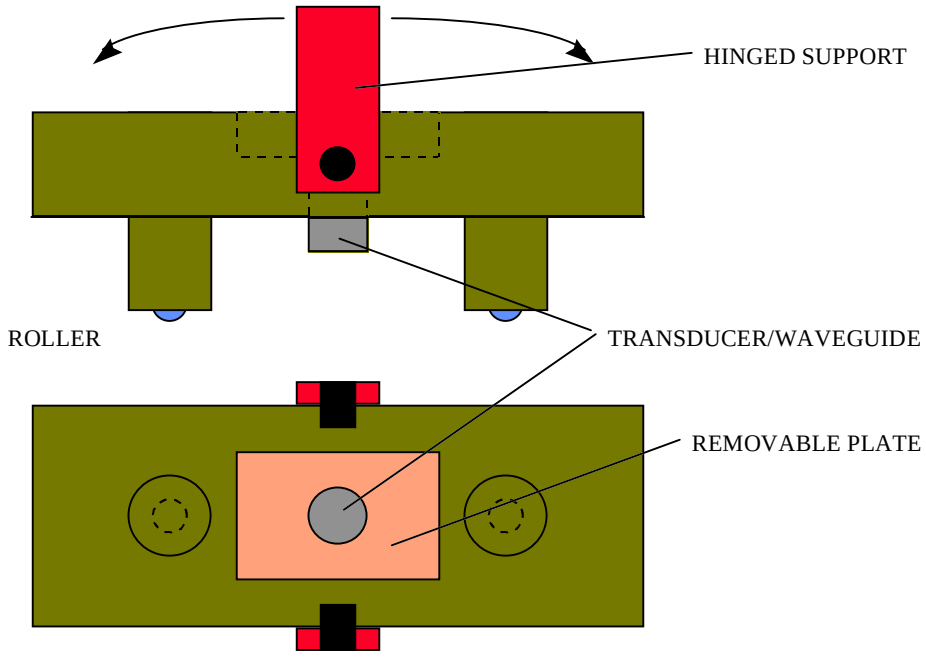

Figure 40. A diagram of the scanning unit. Alumina spheres will be used as rollers to track along the contour of the radome, thus positioning the scanning unit correctly with respect to the radome.

The system will be run via a computer that controls the positioning of the radome/scanner, the collection of data and the manipulation of the data. The computer will scan axially while stepping in the rotational direction. This is done to simplify dome positioning as well as data storage. The scanning unit will move along the length of the dome and collect data at the specified step size. After scanning the entire length, the radome will be rotated through an arc which will cause the base of the radome, which has the greatest circumference, to travel one step and then the scanning unit will move to the other end of the dome, collecting data on its way. Because the circumference of the radome decreases, the effective step size in the rotational direction will be less at the tip than at the base. The data will be stored in a rectangular array and then compressed using a sliding window averaging algorithm to account for the change in circumference. The resulting array will be triangular and more representative of the radome shape. A skilled operator is required to configure the scanning software in order to obtain meaningful images.

Scans will be displayed on a monitor and can be printed. Scans of smaller regions of interest can also be made at higher resolution if desired. Porosity can be obtained from the velocity of sound in Zr-PBSN which can be determined at any point on the radome by first moving the ultrasonic transducer over the desired location and then obtaining the time between the front and back wall reflection from the oscilloscope display. This time along with the thickness of the dome can be used to determine the velocity of the wave through the material. This velocity can then be directly transformed into a porosity value.

The proposed system will evaluate radomes by ultrasonic C-scanning using a pulse-echo configuration. The radome will be supported by rollers and will be positioned by rotating the dome as well as adjusting the position of the scanning unit. A computer will be used to control positioning, data acquisition and data manipulation. The scanning

unit has interchangeable plates to accommodate different transducers and evaluation methods.

CONCLUSION

Advances in aerospace technology have led to missiles and planes that fly higher, farther and faster, fueling a need for new materials that can withstand greater physical demands. Conventional radome materials such as slip cast fused silica and Pyroceram 9606™ ($2MgO \cdot 2Al_2O_3 \cdot 5Sio_2$, cordierite) are no longer capable of surviving the harsh physical environment of the latest radar-guided tactical missiles. A replacement material has been developed that is stable up to 1400°C, has a low and thermally stable dielectric constant, low coefficient of thermal expansion and high thermal shock and rain erosion resistance. This material, Zirconium phosphate bonded silicon nitride (Zr-PBSN), developed at the Naval Surface Warfare Center, also offers a low cost processing method based on pressureless sintering. This material promises to be a significant improvement over conventional radome materials, but the manufacturing process has yet to be qualified. Defects in radomes often result in catastrophic failure, therefore a system for nondestructively evaluating (NDE) radomes is required.

Conventional radomes have been inspected with visible methods, including die penetrants, which work well for detecting surface flaws. Zr-PBSN processed by the pressureless sintering method will have inherent porosity between 15% and 20%. Although this porosity decreases strength and alters the dielectric characteristics of the material, it is acceptable within certain limits. Visible inspection methods can not effectively detect variations in porosity so a method that can must be found. It was desired that the new NDE system detect all possible flaws that could arise in Zr-PBSN radomes including cracks, delaminations, voids, impurities as well as porosity. Other considerations included ease of use, reliability, cost and time of inspection.

The first step in evaluating candidate NDE methods for a radome evaluation system was to make Zr-PBSN samples with intentionally fabricated flaws so each method's ability to

detect various flaw types could be determined. The samples were flat discs two inches in diameter and roughly half an inch thick. Flaws included impurities, surface cracks, delaminations, voids and porosity variation. Some samples obtained additional flaws, usually cracking or delamination, due to the implanted defects. Several small handmade radomes were attempted, but only one survived the process. This radome was made to be flawless, but several surface cracks and a burst-type flaw resulted. A number of one inch diameter discs were fabricate with varying porosities. Porosity was varied by adjusting the cold iso-static pressing (CIP) pressure or by the addition of very fine graphite powder, which burned off upon firing.

Transmitted light methods were attempted using both visible and infrared wavelengths. No light was observed to be transmitted by the Zr-PBSN, but it was noted that, when heated from the inside by a light bulb, the surface temperature varied on the small dome. It was thought that internal defects were disrupting the heat flow from the inside of the radome to the surface, thus causing the uneven heating which was detected by the IR camera. Thermal analysis was attempted with the discs by creating a heat flow and looking for changes in that heat flow caused by the embedded defects. It was found that things like delaminations and high porosity hindered the heat flow, but vertical cracks and small defects far from the surface were very hard to detect. Neither transmitted light nor thermal analysis was considered acceptable as Zr-PBSN radome NDE techniques.

Ultrasonic inspection was performed by C-scanning with a 15 MHz 0.25” diameter focused transducer in the pulse-echo configuration using water as a couplant. This method proved adept at detecting all of the fabricated defects and the diameter of the sound energy resulted in very small defects being magnified on the resulting scan images. Areas of high porosity attenuated the sound energy slightly and were visible in the scans as regions of low intensity. The porosity of each one inch disc was determined by the Archimedes method. The velocity of a longitudinal elastic wave was determined

in each sample by measuring the time between the front surface reflection and the back surface reflection with the ultrasonic equipment and dividing by the distance traveled. A correlation between velocity and porosity was obtained by testing appropriate models found in the literature. If a region of porosity is found while scanning, then the velocity can be determined at the region of interest and the correlation can be used to quantify the porosity. Ultrasonic C-scanning was chosen as the best NDE method for evaluating Zr-PBSN radomes.

A scanning fixture has been proposed. Ultrasonic inspection requires a couplant to facilitate wave propagation between the transducer and the radome. Water has little long term affects on the material and is an effective couplant. The scanning fixture will consist of a cradle within a tank. The radome will lay horizontally on the cradle which has rollers that will rotate the radome while scanning. A scanning unit will be suspended overhead by a rail-table and will mechanically orient the transducer so that it is perpendicular to the radome surface while scanning axially. A computer will be used to control all motion, data acquisition and data manipulation.

REFERENCES

1. I.G. Talmy, C.A. Martin, D.A. Haught, and A.E. Janovsky, "Phosphate Bonded Silicon Nitride Ceramics for Advanced Radome Applications," *Proc. 5th DoD Electromagnetic Windows Symp.*, Boulder, Colorado, October 20, 1993.
2. I.G. Talmy, C.A. Martin and A. H. Le, "Phosphate Bonded Non-Oxide Ceramics," *private communication.*
3. I.G. Talmy, C.A. Martin, A.E. Janovksy and A. Le, "Processing of Silicon Nitride Ceramics Using Phosphate Bonding Techniques," *Proc. 16th Conf. on Metal Matrix, Carbon and Ceramic Composites*, NASA CP-3175, 1, 221-230 (1992).
4. I.G. Talmy and C.A. Martin, "High Temperature Properties of Phosphate Bonded Ceramics," *private communication.*
5. I.G. Talmy, C.A. Martin and D.A. Haught, "Phosphate Bonded Si_3N_4 and AlN Ceramics," *private communication*.
6. I.G. Talmy, C.A. Martin, S. Dallek, A.E. Janovsky and D.A. Haught, "Environmental Stability of Phosphate Bonded Silicon Nitride Ceramics," *Proc. 17th Conf. on Metal Matrix, Carbon and Ceramic Composites*, NASA CP-3201, (1993).
7. R.M. Spriggs, *J. Amer. Ceram. Soc.* 44, 628 (1961).
8. D.P.H. Hasselman, *J. Amer. Ceram. Soc.* 57, 452 (1962).
9. B.O. Aduda and R.D. Rawlings, *J. Mater. Sci.* 29, 2297 (1994).
10. M.R. Stinson and Y. Champoux, *J. Acoust. Soc. Am.*, 91, 685 (1992).
11. J. Allard, P. Herzog, D. Lafarge and M. Tamura, *Applied Acoustics*, 39, 3 (1993).
12. K.K. Phani and S.K. Niyogi, *J. Mater Sci.*, 22, 257 (1987).
13. J.C. Wang, *J. Mater. Sci.* 19, 801 (1984).
14. M. Kukpova, *J. Mater. Sci*. 28, 52065 (1993).

APPENDIX

SAMPLE PREPARATION

All samples were constructed following the methods developed by the Ceramics Group at the Naval Surface Warfare Center (NSWC) at White Oak, MD. A list of materials can be found in Table 1. All samples were made using grade E101 Zirconia, which had the greatest surface area to mass ratio. The other two grades (760/1 and 762/1) were used to compare the effects of Zirconia particle size on residual Zirconia after processing.

Table 1. A list of chemicals, grades and manufacturers used to produce Zr-PBSN samples.

MATERIAL	GRADE	SUPPLIER
Si_3N_4	**LC-12S**	**H.C. STARK** **45 INDUSTRIAL PARK** **NEWTON, MA 02161** **617-630-5800**
ZrO_2	**E101** **XZO 760/1** **XZO 762/1**	**MEI** **500 BREEZE RD.** **FLEMINGTON, NJ 08822** **908-782-3300**
H_3PO_4 85% Aqueous Sol.	**TECHNICAL GRADE**	**RHONE POULENC BASIC CHEMICALS** **ONE CORPORATE DR.** **BOX 881** **SHELTON, CT 06484** **203-925-3300**

Samples were constructed to have a composition of 75 vol% Si_3N_4 and 25 vol% ZrP_2O_7. Table 2 contains information on the amounts of each chemical used to achieve this composition. The reaction between Zirconia and phosphoric acid, which occurs at 250°C, is show in equation (1).

$$ZrO_2 + 2(H_3PO_4) \leftrightarrow ZrP_2O_7 + 3(H_2O) \quad (1)$$

Powder was mixed in small batches that resulted in approximately 10 cubic centimeters of Zr-PBSN after evaporation of water upon heating.

Table 2. Chemical amounts used to make Zr-PBSN composition of 75 vol% Si_3N_4.

CHEMICAL	AMOUNT USED PER BATCH
Si_3N_4	**23.87 g**
ZrO_2	**3.65 g**
H_3PO_4 (85% Aq. Sol)	**6.82 g**

A clean mortar and pestle was used to first mix all of the Zirconia and phosphoric acid resulting in a white pasty mix. Silicon nitride was gradually mixed with the mortar into the Zirconia-phosphoric acid mix until all of the silicon nitride had been added. The result was a gray gummy powder. The resultant mixture was sieved twice with a 500 micron screen resulting in a granulated gray powder. The powder was immediately sealed in a zip-lock bag to eliminate any water absorption by the powder mix.

Two sample types were constructed. Discs that were 5.08 cm in diameter and roughly one centimeter thick (Fig. 1), and radomes that had in inner diameter of 7.5 cm at the base, a wall thickness of roughly 3 mm and a height of 16 cm (Fig. 2). The discs were purposely constructed with flaws that were considered likely to arise during radome manufacture so that each NDE methods abilities' to detect these flaws could be evaluated. The radomes were constructed to test each NDE methods ability to deal with the radome geometry. Attempts to construct radomes with and without defects were made.

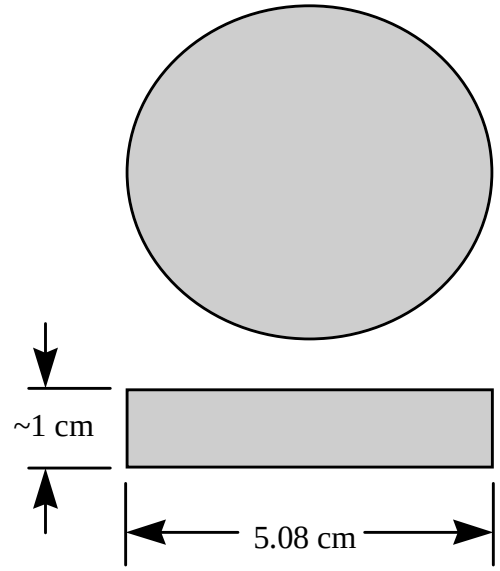

Figure 1. The dimensions of the disc type samples.

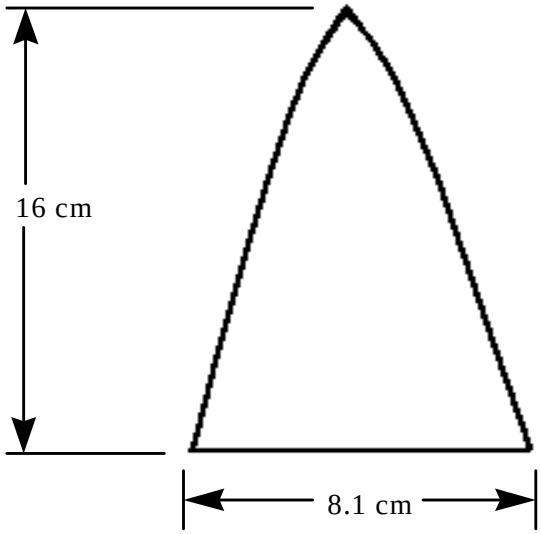

Figure 2. The dimensions of the hand-made radomes.

Discs were made using a 5.08 cm diameter die. The mold consisted of a cylinder, an aluminum plug and a steel die. All parts that contacted powder were first thoroughly cleaned, dried and then coated with mold release. Powder was poured onto the plug, which floated within the cylinder. The top of the powder surface was leveled and small holes roughly 2 cm deep were made with the wooden end of a cotton swab (about 2 mm

in diameter) and finally the die was inserted into the mold (Fig 3). Care was taken to lower the die slowly into the cylinder to minimize powder being blown up into the space between the die and the mold by the escaping air. The powder was then bi-directionally die pressed at 600 Kg/cm^2. Force was applied gradually until the desired pressure was achieved and reapplied until compression ceased. Pressure was maintained for thirty seconds and then released over a period of one minute. This process was then repeated. The resulting green ceramic disc was carefully removed from the mold. If the die press pressure was too great phosphoric acid squeezed out of the powder, which was noticeable after removal from the mold. This resulted in material that, after firing, was mechanically inferior to correctly processed Zr-PBSN material.

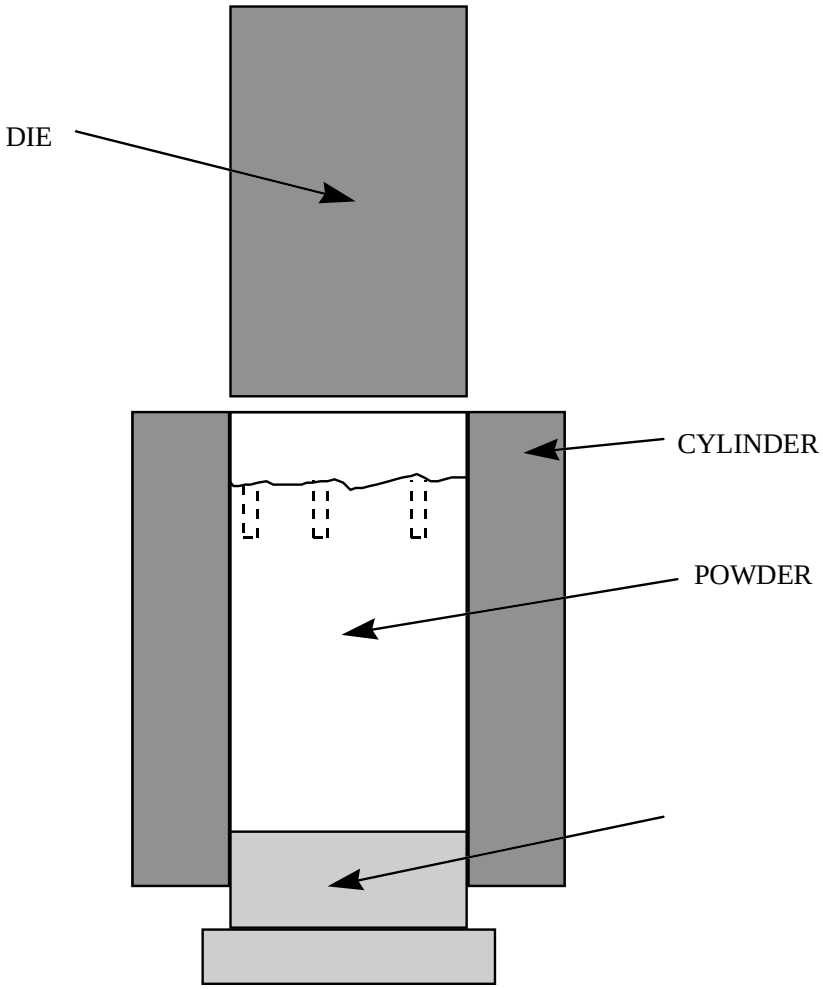

Figure 3. The mold and die setup for disc making.

The next step was to Cold Iso-static Press (CIP) the green ceramic disc. The disc is first inspected for any flaw that may have occurred in the die-pressing process. Often the disc will partially delaminate when pressure is released from the mold, or the disc may partially stick to the die and separate upon removal. If the disc is found to be satisfactory, it is then vacuum-bagged in a nitrile rubber glove. Latex material can not be used because it will absorb the oil used in the iso-press and fail during CIP. The disc and glove are then vacuum-bagged again using the same type of glove. The double vacuum-bagged sample was then CIP at 414 MPa. Pressure was held for thirty seconds and then very gradually bled off over the span of one minute.

The sample was left vacuum-bagged until it was ready to fire to minimize water absorption by the green ceramic. The firing process was critical in avoiding damage caused by thermo-volumetric changes that occur when H_2O evolves during the formation of ZrP_2O_7. The green ceramic is brought from room temperature to 350°C at a ramp rate of 6°/hour. This is the step where ZrP_2O_7 is formed and ramp rates higher than this could result in damage to the sample. The ceramic was then taken to 900°C at a ramp rate of 100°C/hour. It was held at this temperature for 5 hours and then allowed to return to room temperature at a ramp rate of 100°C/hour. The fired ceramic disc was then inspected for damage.

The powder used for making the dome specimens was prepared the same as described above. The mold used to form the dome shape consisted of an aluminum mandrel that provided the inner shape of the dome and a flexible rubber boot with an opening at the top. The mandrel was coated with a thin layer of phenolic resin to protect the aluminum from the phosphoric acid present in the powder. The mandrel and boot were thoroughly cleaned and dried. All surfaces that contacted powder were first coated with mold release and then coated with graphite powder to further aid in removal after CIP.

Vacuum greased was applied around the base of the mandrel and the boot was then attached by wrapping multiple rubber bands around the base (Fig 4). Care is necessary to make sure that the boot is centered on the mandrel. This can be done by sighting down the top of the hole in the boot and making sure that the tip of the mandrel is exactly in the center of the hole.

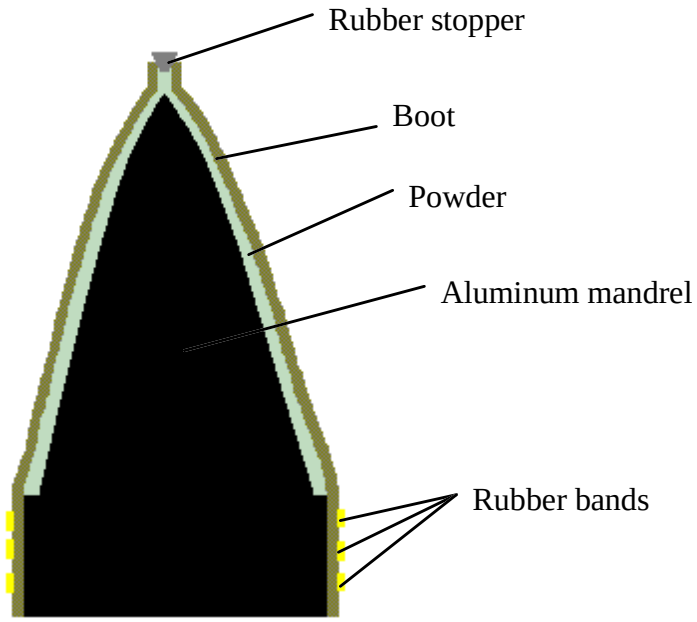

Figure 4. A cross-section of the radome molding setup.

A semi-stiff wire cage was placed over the boot to help the mold keep its correct shape as powder was added. A funnel was fashioned from construction paper and placed in the opening of the boot to aid the pouring of powder into the mold. The mold was placed on a vibrating table to aid packing of the powder as it was poured. At regular intervals during the pouring process, the powder was hand packed by squeezing the boot around its circumference as evenly as possible. If the powder completely filled the boot it was hand packed again until no more powder could be added to the mold. After the mold was filled, graphite powder was poured into the top and the packed down by a rubber stopper. The stopper was secured by rubber bands and then the finger of a nitrile glove

was placed over the opening and secured with rubber bands. This package was then CIP at 414 MPa which was held for thirty seconds and then bled off over a time of one minute.

All rubber bands were then cut and the boot was then removed with extreme care especially in regards to the dome tip. Assuming that the dome has survived relatively intact, final shaping is done by hand sanding with 100 grit sand paper. It is important to keep the sandpaper relatively free of powder as it will cause large chunks of the dome to fall off if the paper is packed with powder. Once the final shape is achieved, reduce grit size until a final pass is made with 600 grit cloth. Extreme caution was used when handling a green dome. The material was very fragile and tended to chip on the edges. The dome was fired with the same heat treatment used for the discs.

VITA

Jonathan Medding grew up in the town of Amesbury, Massachusetts. He lived there on a small lake until the age of eleven. Growing up in proximity to the lake he learned to enjoy swimming, sailing, water skiing as well as ice skating in the winter. At age eleven, he moved a short distance away to the rural town of West Newbury. While living there, he graduated from Pentucket Sr. High School, ranked #7 out of 157 students. In high school he lettered in Soccer and Tennis received the Most Improved Player award for both teams his senior year. Jonathan applied and was accepted to the Aerospace Engineering programs at Georgia Tech, University of Colorado in Boulder, Rensalear Polytechnic Institute and Virginia Tech in Blacksburg. Virginia Tech was the ultimate winner due to financial benefits including low tuition and the Marshal Hahn Engineering Scholarship as well as Blacksburg's small college town atmosphere.

Freshman year in Blacksburg included two major events for Jonathan. The first was academic, being a decision to pursue Materials Engineering instead of Aerospace Engineering. The second was a decision to participate in the Ski Team of Virginia Tech where Jonathan made many of his strongest friendships. While completing his undergraduate degree, Jonathan participated in the COOP program by working in the Locomotive Shop of Norfolk Southern in Roanoke, Virginia. This experience was a strong complement to the knowledge gained in academia and many real life lessons were learned. Upon graduation from Virginia Tech in may of 1994, Jonathan spent the summer in Blacksburg working to save money for a trip to Costa Rica. After spending five weeks in the Central American country surfing and learning Spanish, Jonathan returned to his Massachusetts home shortly before Christmas.

Jonathan loaded his belonging in his truck and then proceeded to drive to Seattle, Washington by way of Blacksburg, New Orleans, Albuquerque and Durango Colorado.

The dismal job market in Seattle led to a return to Virginia Tech for an M.S. in Materials Science. Working for Dr. J.C. Duke, Jr., Jonathan worked on a project involving nondestructive evaluation of ceramic radomes, that was sponsored by the Navy. Jonathan Completed his Masters in December of 1996 after a year and a half in graduate school and is pursuing a career in semi conductor processing.

Jonathan Medding